Timing constraints on building an intermediate plutonic arc crustal section: U- Pb zircon geochronology of the Sierra Valle Fértil–La Huerta, Famatinian arc, Argentina

Mihai N. Ducea,[1] Juan E. Otamendi,[2] George Bergantz,[3] Kelley M. Stair,[1] Victor A. Valencia,[1] and George E. Gehrels[1]

Received 18 September 2009; revised 11 January 2010; accepted 22 January 2010; published 13 July 2010.

[1] The Sierra Valle Fértil Range in northwestern Argentina exposes a tilted crustal section through the Ordovician Famatinian arc, from >25 km to shallow crustal paleodepths. Fourteen new U-Pb zircon crystallization ages of magmatic rocks from Sierra Valle Fértil area show that this section of the arc was built over a short time interval during the Ordovician, between 485 and 465 Ma. Zircon rim ages demonstrate that high-grade metamorphism and migmatization were synchronous with magmatic emplacement. Inherited ages in some of the plutonic rocks as well as detrital zircons in the metasedimentary framework suggest that the Famatinian arc was emplaced into a thick miogeoclinal cover to the thinned margin of the proto-South American continent in the Ordovician, which represents a part of Gondwana. Docking of the Precordilleran terrane outboard of proto-South America led to the cessation of arc magmatism in the Valle Fértil area and preservation of the arc in its early stages after <60 Myr of subduction during the Pampean and Famatinian magmatic stages. Our age data from the Sierra Valle Fértil indicate that wet mafic magmas were emplaced into the section at a rate typical for modern island arcs, ~30 km^3 km^{-1} Myr^{-1}. The production of intermediate to felsic magmas in the upper plate was a result of partial melting of the metasedimentary framework and hybridization with mantle-derived melts and resulted in the generation of tonalites, granodiorites, and granites in the upper crust at a rate of ~100 km^3 km^{-1} Myr^{-1}, similar to major magmatic flare-ups in the mature arcs of North American Cordillera. The Sierra Valle Fértil arc section is a type example of an immature Cordilleran arc, before major crustal thickening and crustal overturn takes place in the upper plate. The Famatinian arc section may also be an equivalent to the crustal architecture of more mature modern island arcs, such as parts of the Aleutians, Caribbean, and Japan. **Citation:** Ducea, M. N., J. E. Otamendi, G. Bergantz, K. M. Stair, V. A. Valencia, and G. E. Gehrels (2010), Timing constraints on building an intermediate plutonic arc crustal section: U- Pb zircon geochronology of the Sierra Valle Fértil–La Huerta, Famatinian arc, Argentina, *Tectonics*, *29*, TC4002, doi:10.1029/2009TC002615.

1. Introduction

[2] Intermediate composition magmas produced at continental magmatic arcs [*Armstrong*, 1988] reflect a complex combination of addition of new crustal material and recycling of continental crust by multiple mechanisms [*Hamilton*, 1981; *Pitcher*, 1993; *Davidson and Arculus*, 2006; *Lipman*, 2007]. The mass budget of overall crustal growth versus recycling in arcs over geologic time is yet to be firmly quantified but several mechanisms [e.g., *von Huene and Scholl*, 1991] have positively been identified in modern and ancient arcs [*Greene et al.*, 2006; *Klepeis et al.*, 2003; *Jagoutz et al.*, 2007]. Crustal growth occurs via mafic magmatic additions from the mantle wedge and in some instances the downgoing oceanic plate, to which rocks with longer residence in the crust can be added via melting of the subducted sedimentary package, melting of tectonically underplated fore arcs, and/or melting of the upper plate. Elemental and isotope geochemistry can sort out these mechanisms in some cases [*DeBari*, 1997; *Beard*, 2008; *Lackey et al.*, 2008; *Zeng et al.*, 2005] but cannot unambiguously resolve among these different mechanisms of crustal mass addition and recycling. A more tractable approach to resolving material balance in magmatic arcs is to characterize the tempo of melting [*Ducea*, 2001], and to correlate changes in magmatic flux over time with regional geological processes [*DeCelles et al.*, 2009; *Ducea et al.*, 2009]. Recent studies have addressed this questions in various island and continental arc settings [e.g., *Calvert et al.*, 2008; *Jicha et al.*, 2006, 2009] and it is becoming increasingly clear that many arcs have spikes of high magmatic flux events separated by lulls and these changes in tempo can be attributed to either to regional tectonic processes [*DeCelles et al.*, 2009] such as foreland shortening, fore-arc subduction, terrane accretion, lower crustal and lithospheric mantle foundering (delamination), or to changes in plate kinematics parameters during subduction. As a result, most long-lived continental arcs are subject to multiple high-flux events, recycling of earlier magmatic products and crustal overturn beneath large volcanic centers.

[1]Department of Geosciences, University of Arizona, Tucson, Arizona, USA.
[2]Departamento de Geología, Univesidad Nacional de Río Cuarto, Río Cuarto, Argentina.
[3]Department of Earth and Space Sciences, University of Washington, Seattle, Washington, USA.

0278-7407/10/2009TC002615

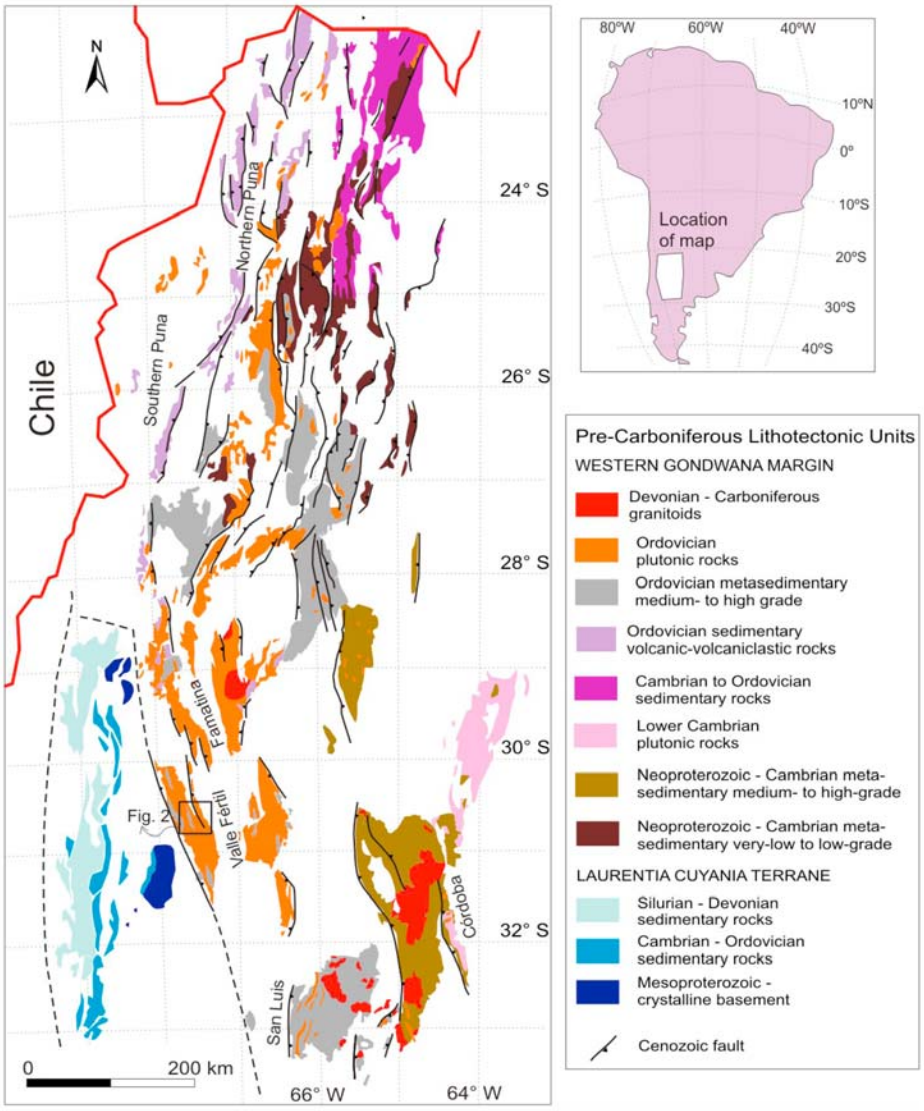

Figure 1. Geology of the central segment of the Famatinian arc in northwest Argentina, showing tectonic boundaries and geographical features referenced in the text.

Crustal overturn is a relatively new concept in arc magmatism and refers to the ability of partially molten lower arc crust or batches of felsic magmas to rise adiabatically [*Babeyko et al.*, 2002; *Depine et al.*, 2008] as large sheets at the expense of downgoing (sinking) framework rocks and older plutons beneath kinematic frontal arcs such as the western Cordillera of the modern Andes, or the ancient Sierra Nevada. Consequently, baseline, mantle-derived magmatic fluxes and compositions are difficult to isolate from other superimposed parameters.

[3] Little is known about fluxes of mafic and intermediate magmas in the initial stages of continental arc magmatism, before complexities mentioned above start playing an important role in redistributing mass available for partial melting. Are mafic fluxes in juvenile continental arcs similar to those in oceanic arc settings? Do felsic high-flux events take place in such settings, and if yes, on what time scales?

[4] The Sierra de Valle Fértil–La Huerta is a continental basement block in the modern Sierras Pampeanas, northwestern Argentina [*Jordan and Allmendinger*, 1986], representing an intact tilted crustal section that exposes a portion of and early Paleozoic magmatic arc [*DeBari*, 1994] from paleodepths of over 25 km to shallow upper crustal levels [*Otamendi et al.*, 2008] (Figure 1). The Sierra de Valle Fértil–La Huerta is a "static arc" in which the entire exposed crustal section lacks evidence for synemplacement regional deformation. The arc was emplaced into a regionally significant but rather uniform sedimentary sequence of possible passive margin origin (the Puncoviscana Formation). The arc shut off some 60 Myr after its initiation by the accretion of the Precordilleran terrane to the western margin of Gondwana during the late Ordovician [*Thomas and Astini*, 1996; *Astini and Dávila*, 2004; *Ramos*, 2004]. Two separate magmatic events are recognized regionally, the Pampean (Cambrian)

and Famatinian (Ordovician), both of which generated calc-alkaline, arc magmas; they represent most likely a sequence of continuous products resulting from subduction along the proto-South American margin (of Gondwanan origin).

[5] The preserved Famatinian arc is a continental arc frozen into its earlier stages of development, before the development of thick crust on the upper plate, in contrast to most of the extinct arcs of western North America. Moreover, the accretion of Precordillera (also known as Cuyania) was a "soft" event at the latitude of the Sierra de Valle Fértil–La Huerta, an event that did not lead to collision-related metamorphism of the Famatinian arc-related rocks but only tilted the Famatinian arc on its side [*Thomas and Astini*, 1996]. The combination of tilting, lack of postarc metamorphism and tectonism, simplicity of end-members, and the great exposures in the arid Sierra Pampeanas make the Sierra de Valle Fértil–La Huerta one of the best arc exposures worldwide.

[6] Field observations and previous geochemical work show that hybridization in the upper plate played an important role in generating all arc products in the Sierra de Valle Fértil–La Huerta [*Otamendi et al.*, 2009a, 2009b]. Magmatic hybridization in the upper plate of this former subduction system generated the entire diversity of the arc products. At middle paleocrustal depth the arc consists mostly of two intermediate compositions: quartz diorite and tonalites, whereas, the upper crust of the paleoarc sequence is made up by granodioritic to granitic plutons.

[7] The Sierra de Valle Fértil–La Huerta provides a unique opportunity to decipher the evolutionary history and tempo of a static arc. U-Pb zircon geochronology data reported below constrain the timing of crystallization, arc metamorphism, and tectonic history through inheritance (see Data Set S1 in the auxiliary material).[1] We use laser ablation-multicollector-inductively coupled plasma-mass spectrometry (LA-MC-ICP-MS) techniques to determine U-Pb zircon ages of the main rock units in the Valle Fértil region, to show that a high-flux event of <20 Myr is responsible for entirely rebuilding the regional crust through progressive accumulation of mafic arc magmas at a midcrustal neutral density level and hybridization with local framework rocks, without the aid of deformation in the upper plate. In contrast, mature Cordilleran arcs (e.g., the Mesozoic– early Cenozoic batholiths of North America or the modern Andes) are "dynamic" arcs in that evolve in close connection with upper plate tectonic events [*Armstrong*, 1988; *Ducea*, 2001, 2002; *Ducea and Barton*, 2007; *Saleeby et al.*, 2003; *Gehrels et al.*, 2009].

2. Geologic Setting

[8] The Sierra de Valle Fértil–La Huerta area is a 100 km long mountain range within the Sierras Pampeanas region. The uplift of the Sierras Pampeanas took place within the past few million years and continues today; these ranges are basement-cored uplifts similar to those formed during the Laramide within the continental interior of western North America as a result of shallow subduction and presumably increased coupling between the subducting and upper plates. Indeed the Sierras Pampeanas ranges are located above a shallowly subducting (in places flat) slab within the framework of the modern central Andes. The magnitude of shortening is minimal and most ranges are bounded by steep active faults with little recent/modern internal deformation.

[9] Basement rocks exposed throughout the Sierras Pampeanas region paint a complex tectonomagmatic sequence of events that span the latest Proterozoic to the late Paleozoic. Shortening (orogenic), accretion and magmatic events developed along an active margin that formed along Gondwana's margin regionally expressed by the Rio de la Plata craton (Figure 1) [*Ramos*, 2008]. The proto-Andean margin of western Gondwana has experienced fairly continuous subduction with relatively short interruptions during terrane accretions [*Cawood*, 2005] since the latest Proterozoic–early Paleozoic. The Pampean Orogeny was built on the once active margin of the Rio del La Plata craton when subduction began at circa 550 Ma [*Rapela et al.*, 1998; *Schwartz et al.*, 2008]. Although sometimes referred to as a "terrane" or orogenic event, the Pampean orogeny is more likely a time of continental arc magmatism built in place along the continental margin, with some associated deformation. Subduction-related magmatic activity paused between circa 525 and 495 Ma, stepped out to the west and resumed on the western margin during the growth and evolution of the Famatinian magmatic arc [*Pankhurst et al.*, 1998]. The lack of subduction-related magmatism during the late Cambrian was caused by either accretion of the Pampean terrane to the proto-Pacific Gondwanan margin [*Rapela et al.*, 1998], a ridge-trench collision on the border of the Gondwanan landmasses [*Schwartz et al.*, 2008], or other unresolved mechanism. The nature of the Pampean Orogeny remains still a controversial issue. Current understanding, however, shows that the Pampean thermotectonic orogeny was short lived (circa 530–515 Ma) and affected thick Neoproterozoic–early Cambrian sedimentary sequences [*Piñán-Llamas and Simpson*, 2006; *Martino et al.*, 2009; *Drobe et al.*, 2009]. These thick mostly marine sedimentary sequences that are regionally referred to as "Puncoviscana Formation" were deposited in basins along the proto-Pacific margin of the western Gondwana [e.g., *Ježek et al.*, 1985]. It is unclear as to whether the Puncoviscana rocks are passive margin accumulations, are turbidites formed during subduction times, or represent a regionally significant rifting event, as the tectonosedimentary study of this extensive package is still in its infancy [*Ramos*, 2008]. As an end result of the almost continuous Phanerozoic tectonism, the Pampean Orogen now makes a N–S trending belt from southern Córdoba (~33°S) into southern Bolivia [*Aceñolaza*, 2003; *Drobe et al.*, 2009] (see also Figure 1).

2.1. Famatinian Arc

[10] The Famatinian arc started at circa 495 Ma when subduction was established along the outboard boundary of the Pampean Orogen [*Mulcahy et al.*, 2007] (Figure 1). The southern segment (28°S to 38°S present-day coordinates) of the Famatinian arc was closed during the middle Ordovician (beginning at circa 465 Ma) when a continental microplate

[1] Auxiliary materials are available at ftp://ftp.agu.org/apend/tc/2009TC002615.

rifted from North American Laurentian landmasses collided against the proto-Pacific Gondwana margin [*Thomas and Astini*, 1996].

[11] The Famatinian arc is exposed for >1500 km along the strike of the modern central Andes, and the transition from plutonic to volcanic Famatinian rocks can be followed over large regions in northwestern Argentina [*Rapela et al.*, 1992; *Toselli et al.*, 1996; *Pankhurst et al.*, 1998; *Coira et al.*, 1999]. The deepest plutonic levels of the arc are currently exposed along a roughly N–S striking wide belt extending by about 600 km length between 28° and 33°S (Figure 1), coinciding with the areas where the Nazca plate is subducting at a relatively low angle under South America [*Barazangi and Isacks*, 1976]. In contrast, Ordovician eruptive igneous rocks interbedded with sedimentary rocks are still on the Earth's surface within the Puna–Altiplano region [*Coira et al.*, 1999] and in Sierra de Famatina [*Fanning et al.*, 2004], between 22°S and 28°S. The wall rocks of all the Famatinian plutonic batholiths are supracrustal sedimentary packages largely consisting of siliciclastic sediments with subordinate interlayered carbonate beds, the Puncoviscana Formation and its metamorphic equivalents [*Caminos*, 1979; *Ježek et al.*, 1985]. This regional-scale sedimentary formation experienced metamorphism at a time broadly synchronous with the igneous plutonic activity, under either contact aureole or regional Barrovian-type regimes [e.g., *Pankhurst et al.*, 2000, and references therein]. As shallower levels of the Famatinian paleoarc crust are exposed northward along strike, the nonmetamorphosed to weakly metamorphosed sedimentary stratigraphic units mapped in the Puna and northern Sierras Pampeanas could be correlated to the south [*Aceñolaza et al.*, 2000]. Late Neoproterozoic–early Cambrian thick turbiditic packages and late Cambrian shallow marine sediments are the most likely protoliths to the metamorphic units hosting the Famatinian arc plutonic rocks [e.g., *Aceñolaza*, 2003], whereas epizonal plutons in Sierra de Famatina and neighboring areas intruded into early Ordovician volcano-sedimentary sequences formed during an early magmatic arc stage [*Toselli et al.*, 1996; *Astini and Dávila*, 2004; *Collo et al.*, 2008].

2.2. Sierra Valle Fértil–La Huerta

[12] Within the western belt of the currently exposed Famatinian magmatic arc, the Sierra Valle Fértil contains well-exposed sections showing the transition between middle to upper crustal levels [*Otamendi et al.*, 2009a]. Field and petrologic studies enable us to infer the position of rock units at the time the magmatism was active [*Mirré*, 1976; *Vujovich et al.*, 1996; *Otamendi et al.*, 2009a]. The shallower part of the exposed section corresponds to its eastern boundary, whereas deeper levels of the Ordovician crust are exposed to the west; the section is tilted almost 90 degrees from its original position. From west to east, the lithologic units display a progression toward more felsic igneous compositions. The overall geometry of this section is one of numerous sills of various magmatic units that invaded a preexisting crust from which only highly migmatized residual metasedimentary rocks are found. At the top of the exposed section the sill-like geometry is replaced by larger felsic intrusives that are mapped as larger stocks. The current state of mapping the Sierra Valle Fértil does not allow one to categorically rule out faults that may have repeated or thinned the section, especially close to its western end near the Precordilleran suture; however, no faults or shear zones have been mapped within the area selected for this geochronologic study. The entire Sierra Valle Fértil section was tilted after the arc's demise, but prior to the deposition of Permo-Triassic basalts that are regionally significant and which retain near horizontal flow fabrics where exposed locally. Docking of the Pre-Cordilleran terrane is the most likely cause for block rotation in the area, although this hypothesis has yet to be thoroughly tested [*Mulcahy et al.*, 2007].

[13] The Sierra Valle Fértil section is almost entirely magmatic with minor framework of migmatitic metasedimentay rocks that were metamorphosed and partially melted during magmatism. The bulk chemistry of the framework rocks suggest that they are high grade equivalents to the regionally abundant late Proterozoic Puncoviscana formation, which is a rather uniform thick sequence of miogeosynclinal rocks. There are no discernable stratigraphic relationships and mapping in the area is based entirely on magmatic way up indicators, metamorphic thermobarometry and grouping of broad rocks types into "units" that predominate at various levels, as proposed by *Otamendi et al.* [2009a]. Field relationships and internal features of each unit have been described in detail by *Otamendi et al.* [2009a]; below we summarize the field relationships and petrographic observations that are essential to interpretation of the U-Pb zircon ages of the studied rocks.

2.2.1. Mafic Unit

[14] This unit is dominated by amphibole gabbronorite and orthopyroxene-amphibole-biotite diorite. Mafic and ultramafic olivine-bearing layered bodies of rocks are widespread within the mafic unit. Based on textural evidence and gradational nature of the contacts in outcrop, we interpret them to be cumulates of gabbroic bodies. Cumulate textures in mafic-ultramafic rocks are critical in establishing the original way up in the section. Virtually all cumulate textures in the studied area point to a 90 degrees tilting to the modern western end of the range, and consequently the eastern side of the section being shallower. This observation is consistent with thermobarometric data from *Otamendi et al.* [2009a, 2009b] suggesting an easterly shallowing of the section.

[15] Although mafic rocks preserve pristine noncumulate or cumulate igneous textures from outcrop to microscopic scales, the majority of the gabbroic rocks has granoblastic textures and has a granulite-like appearance. The gabbro is fine grained and dominated by plagioclase + amphibole + orthopyroxene + oxides + apatite + zircon. It is on average 6 km wide in outcrop pattern (which corresponds to an equivalent crustal thickness since the section is tilted vertically) with a maximum width of 12 km. In places it is layered and includes lens-shaped bodies of ultramafic/mafic cumulates of gabbroic troctolite interlayered with amphibole-bearing peridotitic layers. The mafic unit also has a suite of fine-grained sills and dikes. Dikes and sills are typically massive amphibole gabbros. In addition there are orthopyroxene diorites that occur as lens-shaped bodies among the gabbros.

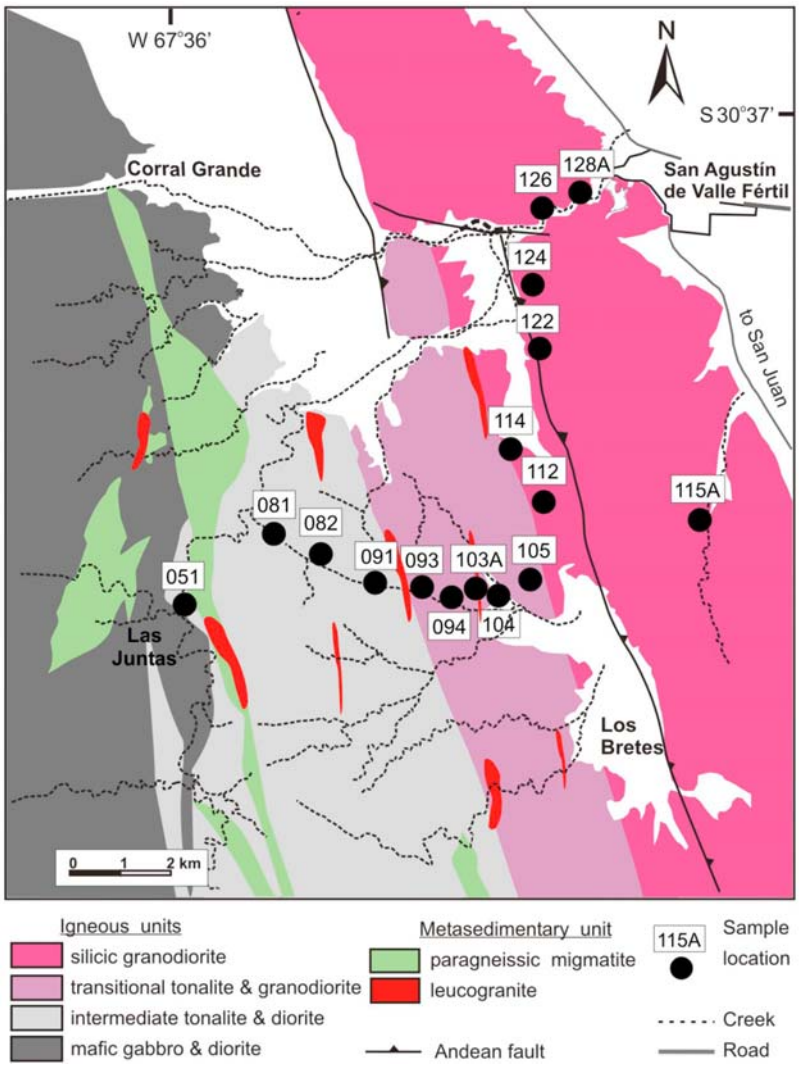

Figure 2. Geologic map of the central section of the Sierra de Valle Fértil (see Figure 1 for location at a regional scale) based on detailed field mapping (this study) and previously published maps [e.g., *Mirré*, 1976; *Otamendi et al.*, 2009a]. Samples dated as part of this study are shown with numbers that are equivalent to full sample's labels, for instance, 051 is for VFKS05-1.

2.2.2. Lower Intermediate Unit

[16] At regional scale, the intermediate unit occurs as elongate belts of intrusions, spreading all over the length of the Sierra Valle Fértil (Figure 2). Tonalites are the predominatant rock types and form elongate sill-like bodies, which are complexly interlayered with igneous mafic rocks and metasedimentary migmatites. The contact between mafic and intermediate units is difficult to estimate at outcrop scale, but where exposed, it appears to be intrusive. Lithologically, this is a heterogeneous unit of biotite-hornblende diorites/tonalites that contain mafic microgranular enclaves, dikes/sills of amphibole gabbros, and metasedimentary septa. Typical quartz diorites and tonalites are medium to coarse grained and are dominated by plagioclase and quartz, with minor amphibole and biotite. Accessory minerals include oxides, zircon, apatite, epidote, allanite, and sphene. In general, diorites and tonalites have a well-defined foliation marked by parallel alignment of tabular plagioclase associated with prismatic amphibole and micas. The elongation of microgranular enclave swarms, the position of tabular mafic sills, and the long side of metasedimentary septa are usually parallel to the primary foliation of tonalites, indicating that all these anisotropies were formed or reoriented under the same strain field. Overall, the foliation and elongation are parallel to the major lithologic units, and are striking approximately N–S.

2.2.3. Transitional Intermediate Unit

[17] The boundary zone separating the tonalite-dominated intermediate unit from a granodioritic silicic batholith is transitional, occupies a 2 km wide belt, and contains a mixture of tonalitic, granodioritic and leucogranitic rocks (Figure 2). Within this transitional zone, the coarse-grained amphibole- and biotite-bearing tonalites dominating the intermediate unit grade eastward to a mixture of

biotite tonalites and felsic leucogranites, which together appear multiply intruded by pod- and dike-like bodies of amphibole gabbros. The lithological transition is marked by an increase in the modal abundance of quartz and biotite in the tonalites. Tonalites in the transitional unit are typically weakly to strongly foliated and contains the same assemblage of accessory minerals as that of tonalites from the intermediate unit. The boundary between the transitional and silicic units is also gradational and located where granodiorites become the dominant rocks, rather than by the first appearance of typical granodiorite.

2.2.4. Silicic Unit

[18] This unit comprises numerous stock-like bodies that together form a typical Cordilleran intermediate to silicic batholith and contains inclusions and dikes/sills of amphibole gabbros. The silicic unit is 5–8 km wide and is dominated by coarse-grained granodiorites, which have either inequigranular or porphyric mineral size aspects. Typical granodiorite has both biotite and hornblende. The inclusions are microdioritic and are a distinctive feature of the granodiorite; these can be found as individual inclusions of tens of meters or as tabular-shaped swarms of multiple inclusions. In addition there are leucogranitic bodies with irregular shapes. A granodiorite of the same composition with a porphyritic texture containing K-feldspar megacrystals is locally the most abundant rock in the silicic unit. Irrespective of the mesoscopic textural variations, most granodiorite include epidote, apatite, sphene, oxide, and zircon as accessory minerals. Granodiorites were intruded at ~2 to 4 kbar, based on preliminary Al-in-hornblende barometry [e.g., *Murra and Baldo*, 2004] consistent with textural observations, and metamorphic framework barometry.

2.2.5. Metasedimentary Unit

[19] This mappable unit is dominated by paragneissic migmatites (metatexite $\gg$ diatexite) that occur as kilometer long belts intercalated with mafic and intermediate igneous rocks. In addition, it occurs as meter long septa within all igneous units. Among metasedimentary rocks, only thick beds of quart-rich gneisses to quartzites do not show any evidence of having experienced partial melting during magmatitic metamorphism [*Otamendi et al.*, 2008]. Instead, most metasedimentary migmatites are characterized by a well-developed layering that results from the alternation of Qtz + Bt + Pl ± Grt ± Crd mesosomes and leucogranitic leucosomes (symbols for minerals after *Kretz* [1983]). Tabular leucogranite bodies ranging in width from 5 cm to tens of meters are found within and outside the metasedimentary migmatites, but have been mapped as part of the metasedimentary unit [*Otamendi et al.*, 2009a]. This unit also consists of subordinate amounts of marble, amphibolite and calcsilicate rocks that locally form kilometer-scale lensoidal bodies within the tonalites and granodiorites. Metapelitic and semipelitic migmatites interlayered in the mafic unit record peak metamorphic pressures between 5.2 and 7.1 kbar at granulite facies temperatures of around 805°C ± 35°C [*Otamendi et al.*, 2008].

[20] Both metatexites and diatexites form this unit dominated by garnet-cordierite-sillimanite migmatitic gneiss from a clastic protolith; however, composition is highly varied on the basis of the sedimentary precursor. It is found in kilometer long strips as interlayered inclusions within the igneous mafic and intermediate rocks. Crosscutting relationships show that supracrustal sedimentary rocks were heated up to granulite facies temperatures and experienced partial melting at the same time as mafic magmatism [*Otamendi et al.*, 2008]. Mesosomes typically include quartz, plagioclase, and biotite with accessory minerals of garnet, cordierite, sillimanite, and K-feldspar. The leucosome is dominated by quartz and K-feldspar with plagioclase, garnet and cordierite. Metamorphic ages coincide with the late phase of arc production 463 ± 2 and 465 ± 4.4 Ma [*Rapela et al.*, 2001; this study].

[21] Spatially associate with metasedimentary migmatites, there are also felsic granites found near the boundary between the mafic, intermediate and metasedimentary units [*Mirré*, 1976] that have been interpreted as magma crystallizing after partial melting and melt segregation from the metasedimentary rocks [*Otamendi et al.*, 2008].

2.3. Crustal Section and Outboard Terrane Docking

[22] The Famatinian arc is a major tectonic feature of South America that extends for over 1500 km along the strike of the proto-South American margin of Gondwana and is exposed, for the most part, to relatively shallow levels of granitic batholiths and surface equivalents. The width of the original arc is difficult to quantify due to complexities associated to post-Ordovician tectonics but is probably around 100 km. For example, Famatinian arc rocks extensively exposed to the north in the Puna region have been affected by Mesozoic extension (informally known as the Salta rift extensional event) and subsequent shortening during Andean compression. Similarly, terrane accretion outboard of the Famatinian arc followed by Permo-Triassic extension regionally significant in the Sierra de Valle Fértil–La Huerta area have modified the original architecture of the arc.

[23] What is clear, however, from our and previous regional mapping, is that the Sierra de Valle Fértil–La Huerta exposes some of the deeper rocks of the Famatinian arc [*Otamendi et al.*, 2009a], and that it appears to be a vertically tilted section from deeper rocks in the west to shallower arc assemblages in the east, without major faults doubling or omitting section. Paleohorizontal indicators are primarily cumulate textures, and they corroborate well with metamorphic equilibration pressures of 0.7–0.8 GPa at deeper levels and progressively shallower exposure levels toward the felsic units, to as low as 0.2–0.4 GPa [*Otamendi et al.*, 2009a]. The Sierra Famatinia to the northeast of the Sierra de Valle Fértil (Figure 1) further exposes shallow intrusives and volcanic rocks of the same arc. The two ranges are separated by a Permo-Triassic extensional basin, and are modestly inverted during recent Andean compression related to flat slab tectonics.

[24] The westernmost exposures of the Sierra de Valle Fértil–La Huerta range may contain some of the deepest arc rock exposures, although geometrically it is clear that they would not exceed paleopressures of 1 GPa. The additional complication in the extreme west area of the range is that it hosts the suture zone (Figure 1) between proto-South America and the Precordillera (Cuyania), a Laurentian terrane docked shortly after the arc's demise. The complicated

Table 1. Summary of Mineral Constitution, Texture, Grain Size, and Fabric for Rocks With U-Pb Zircon Ages

Sample	Rock Unit	Rock Type	Minerals	Observation
VFKS05-1	Mafic	Diorite	Pl-Qtz-Amph-Bt-Ap	Subhedral granular with weak mineral preferred orientation, evidence for semibrittle intragranular and intergranular deformation in Qtz and Pl.
VFKS08-1	Intermediate	Tonalite	Qtz-Pl-Amph-Bt-Mt/Ilm	Coarse-grained subhedral inequigranular.
VFKS08–2	Intermediate	Tonalite	Qtz-Pl-Amph-Bt-Mt-Ap	Medium-grained subhedral granular with local euhedral texture. Weak to marked mineral preferred orientation, subsolidus mineral alignment not reflecting penetrative foliation.
VFKS09-1	Intermediate	Migmatite	Qtz-Pl-Crd-Bt-Sil	Medium-grained, pseudopolygonal granoblastic with crude stromatic fabric.
VFKS09-3	Transitional	Tonalite	Qtz-Pl-Amph-Bt-Mt-Ep	Coarse-grained subhedral inequigranular. Local evidence for nonpenetrative dynamic recrystallization of Qtz.
VFKS09-4	Transitional	Tonalite	Qtz-Pl-Amph-Bt-Mt/Hm-Ep	Coarse-grained subhedral with large Ep crystals mostly around Pl.
VFKS10-3A	Transitional	Leucogranite	Qtz-Kfs-Pl-Bt	Medium-grained anhedral granular. Dynamic recrystallization of Qtz, semibrittle intracrystalline deformation in Pl and Kfs.
VFKS10-4	Transitional	Tonalite	Qtz-Pl-Amph-Bt-Mt/Hm	Coarse-grained subhedral inequigranular with weak mineral preferred orientation.
VFKS10-5	Transitional	Gabbro	Amph-Pl-Mt/Hm-Ap	Coarse-grained subhedral granular with entire igneous fabric.
VFKS11-2	Silicic	Granodiorite	Qtz-Kfs-Pl-Bt-Ep-Hm-Ms	Coarse-grained subhedral inequigranular.
VFKS11-4	Transitional	Tonalite	Qtz-Pl-Bt-Ap-Mt/Hm	Medium-grained subhedral granular.
VFKS11-5A	Transitional	Granodiorite	Qtz-Pl-Bt-Kfs-Ep-Ap-Hm-Aln	Coarse-grained subhedral Kfs-phyric, with Kfs megacrysts (up to 4 cm) that include Pl grains. Dynamic mineral recrystallization of Qtz around Kfs crystals. Ep is secondary to Bt.
VFKS12-2	Transitional	Tonalite	Qtz-Pl-Amph-Bt-Hm-Sph-Ep	Medium-grained subhedral inequigranular.
VFKS12-4	Transitional	Granodiorite	Qtz-Pl-Amph-Bt-Sph-Ep	Coarse-grained subidiomorphic inequigranular. Ep and Sph are large subhedral crystals.
VFKS12-6	Transitional	Granodiorite	Qtz-Pl-Kfs-Bt-Amph-Mt/Hm	Coarse-grained suhedral and euhedral inequigranular. Ep occurs spatially associate to Bt and Amph. Qtz and Kfs tend to be interstitial amount large plagioclase crystals.
VFKS12-8A	Transitional	Granodiorite	Qtz-Pl-Kfs-Bt-Ep-Mt/Hm	Coarse-grained suhedral and euhedral with large zoned Pl crystals. Kfs appears sometimes interstitial among Pl. Ep is abundant and secondary to Pl.

shear zone, mylonites, and apparent mélange of Famatinian and Precordilleran rocks make it difficult to interpret the deepest parts of the crustal section simply from an arc evolution perspective at this point.

3. Methods

3.1. Sampling

[25] In this study we report 16 new zircon U-Pb ages of plutonic and metasedimentary rocks. Sampling was performed on a nearly east–west transect across the Famatinian plutonic section from the central Sierra Valle Fértil, ending to the east close to the town of San Agustin (Figure 2). Studied samples cover a range of rock compositions from a diorite sampled at the top of the mafic unit to a Kfs-porphyric granodiorites obtained close to the contact where the silicic unit is covered by Holocene alluvial fan sediments (Figure 2 and Table 1). In the intermediate, transitional and silicic rock units, samples were chosen to document the lithological diversity and have been categorized accordingly. For this, in the intermediate unit we sampled a metasedimentary septum (VFKS09-1). Within the transitional intermediate unit, we collected a leucogranite tabular body (VFKS10-3A) and gabbroic body (VFKS10-5) because these lithologies are abundant in this position of the plutonic sequence [e.g., *Otamendi et al.*, 2009a]. Since tonalitic lenses with gradational boundary are widespread within the granodiorites from the silicic units, a tonalite (VFKS12-2) was also sampled in the silicic unit.

3.2. U-Pb Geochronologic Methods for Igneous Zircon Analysis

[26] Samples chosen for U-Pb zircon geochronology were prepared and run at the University of Arizona. Samples were crushed and pulverized using a jaw crusher and roller mill. Density separation and sieving to collect grains <350 μm was done using a Wilfley table. Additional density separation was done with methylene iodide and magnetic separation using a Franz magnetic separator. The sample with >90% purity was mounted in epoxy within 1″ diameter rings and sanded down ~40 μm depth to expose zircon interiors. Analysis followed procedures described in detail by *Gehrels*

et al. [2008]. Furthermore, general information about data acquisition and reduction is presented below.

[27] U-Pb geochronology of zircons was conducted by LA-MC-ICP-MS at the Arizona LaserChron Center. The analyses involve ablation of zircon with a New Wave/Lambda Physik DUV193 Excimer laser (operating at a wavelength of 193 nm) using a spot diameter of 25 or 35 μm. The ablated material is carried with helium gas into the plasma source of a GV Instruments Isoprobe, which is equipped with a flight tube of sufficient width that U, Th, and Pb isotopes are measured simultaneously. All measurements are made in static mode, using Faraday detectors for ^{238}U and ^{232}Th, an ion-counting channel for ^{204}Pb, and either Faraday collectors or ion counting channels for $^{208-206}$Pb. Ion yields are ~1 mV ppm^{-1}. Each analysis consists of one 20 s integration on peaks with the laser off (for backgrounds), twenty 1 s integrations with the laser firing, and a 30 s delay to purge the previous sample and to prepare for the next analysis. The ablation pit is ~15 μm in depth.

[28] For each analysis, the errors in determining ^{206}Pb/^{238}U and ^{206}Pb/^{204}Pb result in a measurement error of ~1% (at 2σ level) in the ^{206}Pb/^{238}U age. The errors in measurement of ^{206}Pb/^{207}Pb and ^{206}Pb/^{204}Pb also result in ~1% (2σ) uncertainty in age for grains that are >1.0 Ga, but are substantially larger for younger grains due to low intensity of the ^{207}Pb signal. For most analyses, the crossover in precision of ^{206}Pb/^{238}U and ^{206}Pb/^{207}Pb ages occurs at ~1.0 Ga.

[29] Common Pb correction is accomplished by using the measured ^{204}Pb and assuming an initial Pb composition from *Stacey and Kramers* [1975] (with uncertainties of 1.0 for ^{206}Pb/^{204}Pb and 0.3 for ^{207}Pb/^{204}Pb). Our measurement of ^{204}Pb is unaffected by the presence of ^{204}Hg because backgrounds are measured on peaks (thereby subtracting any background ^{204}Hg and ^{204}Pb), and because very little Hg is present in the argon gas. Interelement fractionation of Pb/U is generally ~20%, whereas fractionation of Pb isotopes is generally <2%. In-run analysis of fragments of a large Sri Lanka zircon crystal (generally every fifth measurement) with known age of 564 ± 4 Ma (2σ error) is used to correct for this fractionation [see *Gehrels et al.*, 2008]. The uncertainty resulting from the calibration correction is generally ~1% (2σ) for both ^{206}Pb/^{207}Pb and ^{206}Pb/^{238}U ages.

[30] The reported ages are determined from the weighted mean of the ^{206}Pb/^{238}U ages of the concordant and overlapping analyses [*Ludwig*, 2003]. The reported uncertainty (labeled "mean") is based on the scatter and precision of the set of ^{206}Pb/^{238}U or ^{206}Pb/^{207}Pb ages, weighted according to their measurement errors (shown at 1σ). The systematic error, which includes contributions from the standard calibration, age of the calibration standard, composition of common Pb and U decay constants, is generally ~1–2% (2σ).

[31] Some of the ages reported below have high mean square weighted deviation (MSWD) values, which suggest they do not represent single, coherent populations. This is especially the case for the older Famatinian ages, which contain Cambrian cores too small to be resolved with the technique employed here. The significance of the relatively high errors is that the real age span of the analyzed rocks may be in fact smaller than reported (see interpretations).

4. Results

[32] Sixteen samples were analyzed for U-Pb geochronology with an average of about 20 zircons from each sample. Zircons were studied optically under a petrographic microscope and with scanning electron microscope (SEM) in backscatter electron mode and cathodoluminscence. The zircons are typically euhedral to suhedral, clear, transparent and vary in size from 50 to 200 μm. Backscatter electron and CL images show that compositional zoning is common.

[33] Data for the main isotopic ratios and calculated ages are reported in Tables 2–6. We chose five samples to be representative of the full data set, as these samples are critical to most arguments being made in this study. Data from all the other specimens are reported in the Electronic Appendix only. Because of the grain size, we were able to probe several spot points per zircon crystal. Thus, in order to investigate core-rim age relationships we typically performed two or three spots per grain in the great majority of the analyzed zircons. Core spots with a "c" at the very end of their names are reported in Tables 2–6.

[34] Since the great majority of the rocks have inherited zircon ages, all the measured data set are plotted on the U-Pb conventional concordia diagrams, even though the mean age is calculated from a restricted cluster of analytical data. By contrast, in some cases the U-Pb age results that were chosen for computing the weighted age are shown separately in U-Pb concordia diagrams. Some representative cathodoluminescence images are included as insets in the U-Pb conventional concordia diagrams.

4.1. Diorite From the Upper Part of the Mafic Unit

[35] Zircon grains were collected from a diorite (VFKS05-1) within the boundary zone between the mafic and intermediate units [e.g., *Otamendi et al.*, 2009b] (Figure 2). This diorite mostly consists of plagioclase (labradorite-andesine), quartz, hornblende, and biotite. Zircon morphology is dominated by prismatic and complexly zoned as the prevalent type (Figure 3a). Zircons from this diorite have a complex cathodoluminescence pattern from a dark dominant interior to a bright outer zone, but both cores and rims have similar U contents averaging around 390 ppm. Th/U ratios measured with the LA-MC-ICP-MS are always higher than 0.3, and most vary over 0.5 and 1.0 and therefore are characteristic of igneous crystallization [e.g., *Hoskin and Schaltegger*, 2003]. Forty-six spots in 27 zircon grains were analyzed by LA-MC-ICP-MS (Table 2). Two grains yielded concordant best ages at around 560 Ma (Figure 3b), this age is interpreted as due to the existence of inherited cores and is typical of the early stages of regional arc magmatism, the so-called Pampean orogeny [*Rapela et al.*, 1998; *Schwartz et al.*, 2008]. The best age determination for this sample is estimated from a coherent group of 15 points with weighted mean ^{206}Pb/^{238}U age of 484.3 ± 7.9 Ma (Figure 3c). Importantly, the pooled 15 spot points show a spread of concordant ages spanning 30 Ma from 510 to 470, implying inherited Cambrian cores. A significant

Table 2. LA-MC-ICP-MS U-Pb Zircon Data for Diorite VFKS05-1

	Concentration			Isotope Ratios						Apparent Ages (Ma)					
Spot	U (ppm)	Th (ppm)	Th/U	$^{206}Pbm/^{204}Pbc$	$^{207}Pb/^{235}U$	± SE (%)	$^{206}Pb/^{238}U$	± SE (%)	Error Correction	$^{206}Pb/^{238}U$	± SE (Ma)	$^{207}Pb/^{235}U$	± SE (Ma)	$^{206}Pb/^{207}Pb$	± SE (Ma)
1r	170	100	0.59	5750	0.5592	3	0.0735	1.0	0.34	457.3	4.3	451.0	10.5	419.0	60.5
2c	606	282	0.46	20752	0.5962	2	0.0765	1.2	0.59	475.2	5.5	474.8	7.7	473.2	36.3
3c	451	235	0.52	15978	0.5589	2	0.0726	1.3	0.59	451.8	5.8	450.8	8.2	446.1	40.4
4c	413	299	0.72	16328	0.5725	3	0.0743	2.6	0.88	461.8	11.5	459.6	10.9	448.6	31.5
5c	439	362	0.82	15372	0.5578	3	0.0726	1.7	0.48	451.8	7.3	450.1	12.6	441.2	67.5
7c	269	199	0.74	77624	0.6506	4	0.0833	1.7	0.43	516.1	8.4	508.8	15.7	476.5	78.4
8r	343	284	0.83	21738	0.6349	3	0.0811	2.6	0.79	502.7	12.5	499.2	12.9	483.0	44.0
9c	561	536	0.96	27402	0.6441	3	0.0818	1.5	0.56	506.8	7.1	504.9	10.4	496.3	47.9
10	368	235	0.64	19354	0.6641	2	0.0843	0.6	0.40	521.8	3.2	517.1	6.5	496.7	32.6
11r	441	255	0.58	18468	0.6441	3	0.0833	0.8	0.28	515.7	4.0	504.9	11.4	456.1	61.2
12	589	391	0.66	24660	0.6316	4	0.0808	4.0	0.93	501.1	19.5	497.1	17.1	478.4	36.1
13c	215	294	1.37	7786	0.6263	3	0.0808	0.5	0.16	500.7	2.4	493.8	12.1	462.0	67.7
14	232	123	0.53	7660	0.6185	2	0.0784	1.3	0.66	486.8	6.2	488.9	7.7	499.0	33.0
15c	345	397	1.15	8768	0.7332	2	0.0903	1.8	0.73	557.4	9.5	558.4	10.5	562.8	36.5
16c	543	447	0.82	9068	0.5856	2	0.0734	1.1	0.60	456.6	4.7	468.1	6.6	524.8	31.0
17c	461	433	0.94	16502	0.6366	2	0.0803	1.0	0.59	497.8	4.7	500.2	6.5	511.0	29.1
19r	211	115	0.55	14136	0.5973	4	0.0765	2.8	0.65	475.0	12.7	475.5	16.1	477.7	71.0
20c	229	73	0.32	13360	0.5922	3	0.0775	1.2	0.40	480.9	5.3	472.3	11.0	430.4	59.4
21	503	167	0.33	36520	0.5949	2	0.0766	1.7	0.84	475.9	7.8	474.0	7.7	465.1	24.2
22c	244	135	0.56	15108	0.6065	4	0.0779	2.2	0.50	483.7	10.2	481.4	16.9	470.1	84.5
23c	331	288	0.87	9624	0.5924	4	0.0756	0.5	0.14	469.5	2.3	472.4	13.4	486.5	77.7
24c	431	367	0.85	4788	0.6457	2	0.0799	1.7	0.75	495.4	8.2	505.8	9.1	553.5	33.4
25	319	233	0.73	6488	0.6176	2	0.0779	0.8	0.38	483.6	3.9	488.3	8.4	510.7	44.0
26c	368	370	1.01	2668	0.5529	4	0.0678	1.5	0.40	423.1	5.9	446.9	13.1	571.2	71.9
27c	526	498	0.95	20472	0.6285	3	0.0805	1.8	0.64	499.3	8.6	495.1	10.9	476.0	47.2
28c	556	558	1.00	2662	0.6255	4	0.0740	2.1	0.47	460.0	9.1	493.3	17.3	651.0	84.2
29	410	255	0.62	19942	0.6463	3	0.0821	1.9	0.75	508.6	9.5	506.2	10.3	495.4	37.9
30c	664	1180	1.78	1928	0.7532	5	0.0858	1.9	0.40	530.4	9.5	570.1	20.2	731.5	89.6
31	424	246	0.58	17892	0.6180	3	0.0787	2.9	0.88	488.4	13.5	488.6	12.6	489.6	34.5
32c	399	249	0.62	17814	0.6372	2	0.0815	1.4	0.60	505.2	6.6	500.6	8.8	479.6	39.3
33	614	402	0.66	27070	0.6615	3	0.0833	2.1	0.81	515.8	10.2	515.6	10.3	514.5	33.0
34c	299	150	0.50	11992	0.6648	7	0.0842	1.0	0.14	520.9	5.0	517.5	28.0	502.8	150.6
35c	556	686	1.23	16568	0.6686	5	0.0824	1.1	0.21	510.5	5.2	519.9	20.5	561.4	107.4
36	455	264	0.58	22658	0.6170	2	0.0794	1.2	0.61	492.7	5.5	488.0	7.2	465.8	32.7
37	281	138	0.49	11926	0.6212	3	0.0789	2.1	0.83	489.5	9.8	490.6	9.8	495.4	31.0
38c	266	202	0.76	11960	0.6544	2	0.0823	1.4	0.70	509.8	6.8	511.2	7.9	517.2	31.1
39	334	155	0.46	15544	0.6453	2	0.0818	1.8	0.86	506.6	8.7	505.6	8.3	501.2	23.4
40c	891	477	0.54	30956	0.6448	3	0.0816	2.7	0.89	505.7	13.1	505.2	12.0	503.1	29.7
41c	416	253	0.61	19692	0.6304	2	0.0804	1.5	0.74	498.7	7.2	496.3	7.9	485.3	29.5
42	365	185	0.51	10674	0.6236	2	0.0804	1.0	0.46	498.4	4.7	492.1	8.3	462.8	41.8
44c	234	154	0.66	10584	0.7287	2	0.0914	0.7	0.32	563.5	3.6	555.8	8.9	524.3	43.0
45c	494	462	0.93	15324	0.5947	4	0.0754	2.9	0.78	468.4	12.9	473.8	13.9	500.3	50.9
46c	190	102	0.54	12540	0.6242	2	0.0796	1.1	0.45	493.5	5.4	492.5	9.7	488.1	49.1
47	262	151	0.58	13048	0.6027	3	0.0787	0.5	0.19	488.1	2.4	478.9	9.9	435.1	56.5
48	134	39	0.30	5668	0.5841	3	0.0770	1.4	0.42	478.0	6.2	467.1	12.0	413.6	65.0
49c	283	183	0.65	3708	0.6441	4	0.0787	1.1	0.25	488.6	5.1	504.8	17.5	579.3	92.6

cluster of 3 core points yielded the youngest best ages between 457 and 451 Ma. Rejection of the rest of the points was made on the basis of large discordance (>10%) on conventional and Tera-Wasserburg concordia diagrams and high error.

4.2. Tonalites From Within the Intermediate Unit

[36] Most zircon crystals are euhedral, prismatic, with the outer thick rim, presumably of magmatic origin (Figure 4a). There are, however, some grains with prismatic habit and well-preserved oscillatory zoning. The presence of inherited cores is most notable in unzoned grains. Almost all zircons present a bright narrow rim. Measured Th/U ratios are higher than 0.5 in the great majority of the zircons.

[37] In the tonalitic sample VFKS08-1, 39 zircon spots were analyzed by LA-MC-ICP-MS. Three grains yielded nearly concordant Mesoproterozoic (Grenvillian) best ages between 1238 and 1127 Ma, likely reflecting core inheritance (Figure 4b). Six additional grains were excluded due to discordance and high error. There is a coherent group of 30 points with apparent concordance and no inheritance with a weighted mean age of 477.4 ± 7.1 Ma (Figure 4c).

[38] In the other typical tonalite (VFKS08-2), we determined 12 spot analyses from eight zircon grains. This data set yielded a coherent group of nine concordant ages with a weighted mean on $^{206}Pb/^{238}U$ ages of 472.3 ± 5.8 Ma. However, the MSWD = 7.2 indicates that the data set did not yield well-constrained spot average (Figure 4d).

Table 3. LA-MC-ICP-MS U-Pb Zircon Data for Tonalite VFKS09-3

	Concentration			Isotope ratios						Apparent Ages (Ma)					
Spot	U (ppm)	Th (ppm)	Th/U	$^{206}Pbm/^{204}Pbc$	$^{207}Pb/^{235}U$	± SE (%)	$^{206}Pb/^{238}U$	± SE (%)	Error Correction	$^{206}Pb/^{238}U$	± SE (Ma)	$^{207}Pb/^{235}U$	± SE (Ma)	$^{206}Pb/^{207}Pb$	± SE (Ma)
1c	258	106	0.41	3323	0.60054	4	0.07541	1.30	0.35	468.6	5.9	477.6	14.2	520.7	76.9
2c	199	164	0.82	8158	1.16426	4	0.12997	3.12	0.87	787.7	23.1	784.0	19.5	773.4	36.6
3r	249	62	0.25	6406	0.66509	5	0.08411	4.52	0.94	520.6	22.6	517.7	19.6	504.9	37.5
4c	1271	1562	1.23	505	0.42372	15	0.06441	1.87	0.13	402.4	7.3	358.7	44.3	84.9	346.1
5	570	602	1.06	448	0.45240	24	0.07434	2.20	0.09	462.2	9.8	379.0	76.2		
6r	233	44	0.19	5316	0.61402	4	0.07878	1.38	0.36	488.9	6.5	486.1	14.7	473.0	78.4
7r	251	86	0.34	7589	0.63554	4	0.07686	2.22	0.54	477.4	10.2	499.5	16.2	602.4	74.7
8r	209	67	0.32	5773	0.62682	3	0.07725	1.80	0.55	479.7	8.3	494.1	12.8	561.6	59.5
9r	264	83	0.32	15116	0.61306	4	0.07807	3.40	0.84	484.6	15.9	485.5	15.5	489.7	47.6
10r	208	111	0.54	3388	0.66886	7	0.08175	3.42	0.49	506.6	16.6	520.0	28.4	579.5	132.1
11c	76	67	0.87	9688	2.02204	3	0.18429	1.74	0.68	1090.4	17.5	1122.9	17.4	1186.5	37.3
12r	359	83	0.23	25791	0.62967	3	0.07883	2.33	0.78	489.2	11.0	495.9	11.8	527.0	41.6
13c	466	230	0.49	19831	0.60347	9	0.07862	5.69	0.62	487.9	26.7	479.4	35.0	439.2	159.7
14r	357	73	0.20	10511	0.60353	4	0.07569	2.14	0.59	470.4	9.7	479.5	13.8	523.3	63.9
15r	263	96	0.36	7904	0.62927	3	0.07762	2.46	0.76	481.9	11.4	495.6	12.7	559.7	45.8
16r	356	146	0.41	8166	0.57507	3	0.07290	1.76	0.70	453.6	7.7	461.3	9.4	499.7	40.0
17r	249	136	0.55	5380	0.59724	2	0.07524	1.00	0.50	467.6	4.5	475.5	7.5	513.5	37.7
18r	436	217	0.50	4215	0.60182	3	0.07770	2.51	0.75	482.4	11.6	478.4	12.8	459.4	49.2
19	275	137	0.50	6301	0.58284	3	0.07568	1.80	0.62	470.3	8.2	466.3	10.9	446.7	50.7
20r	596	437	0.73	4247	0.63807	3	0.08044	2.52	0.91	498.8	12.1	501.1	11.0	511.8	25.5
21c	358	501	1.40	7387	0.61410	3	0.07684	2.37	0.87	477.2	10.9	486.1	10.5	528.3	29.1
22c	546	258	0.47	9978	0.58318	2	0.07492	1.45	0.68	465.7	6.5	466.5	8.0	470.3	34.7
23r	275	148	0.54	1332	0.52985	17	0.07639	1.89	0.11	474.6	8.6	431.7	60.2	209.0	396.3
24	763	609	0.80	4566	0.63002	4	0.08133	1.98	0.56	504.1	9.6	496.1	13.8	459.5	64.3
25r	362	263	0.73	11536	0.58432	4	0.07454	3.77	0.93	463.4	16.9	467.2	15.3	486.0	34.0
26	482	349	0.72	5195	0.61995	4	0.07791	2.14	0.55	483.7	10.0	489.8	15.3	518.7	72.2

4.3. Tonalites Within the Transitional Intermediate Unit

[39] Three tonalitic specimens (VFKS09-3, VFKS09-4, and VFKS10-4) were collected in the plutonic transitional belt where tonalitic rocks are intermixed with leucogranitic and gabbroic rocks (Figure 2) [see also *Otamendi et al.*, 2009a]. The first appearance of typical granodiorites is found on the eastern side of this N–S trending belt. In all of these tonalites the measured U/Th are closer or slightly higher than 1.0. Furthermore, most zircon grains have morphological and cathodoluminescence features typical and characteristic of magmatic growth.

[40] In tonalitic sample VFKS09-3, 28 spots were measured by LA-MC-ICP-MS from 16 zircon grains. This data set yielded a coherent group of 13 apparent concordances and no inheritance with a weighted mean age of 472.9 ± 5.9 Ma (Figure 5a). Two inherited core grains gave Mesoproterozoic and Neoproterozoic ages, respectively. The rest of the U-Pb data were excluded due to discordance (>10%) and high error (>15%).

[41] Thirty-six spots analyses were performed in tonalite VFKS09-4, including 12 core-rim pairs, 10 of single cores and 2 of separate rims. The most remarkable feature of this data set is the well-preserved inheritance (Figure 5b). There is a group of four cores yielding Grenville ages with weighted mean age of 1054 ± 46.4 Ma (MSWD = 2.7 at 2σ). The best constrained Ordovician age is revealed by 11 data that give concordance with a weighted mean on $^{206}Pb/^{238}U$ ages of 474.4 ± 7.9 Ma. The remaining grains yielded ages ranging from the Mesoproterozoic through Neoproterozoic to Early Cambrian, but without any clustering. A large subset of data was rejected from further consideration because of high error (>15%) and deviation, and discordant ages (>10% of discordance).

[42] Thirty spots were analyzed by LA-MC-ICP-MS in tonalitic sample VFKS10-4. Most of them are core-rim pairs. Five points were excluded due to discordance, deviation from the coherent group and high error. Three grains have inherited core Mesoproterozoic ages. The remaining 22 data points yielded a weighted mean $^{206}Pb/^{238}U$ age of 486.4 ± 5.8 Ma (Figure 5c). All tonalites contain zircons with inherited cores that cluster around Mesoproterozoic ages, thus emphasizing the geological significance of continental inheritance from the proto-South American core.

4.4. Other Lithologies in the Transitional Intermediate Unit

[43] A leucogranite (VFKS11-3A) was collected within the transitional zone between the intermediate and silicic units. This type of leucogranite was derived from partially melting and segregation of metasedimentary framework rocks [*Otamendi et al.*, 2009a, 2009b]. Fourteen spot points were measured in zircons. One core grain yielded a $^{206}U/^{238}Pb$ age of 615 Ma, and was found to be outside the main cluster (Figure 6a). The remaining 13 data points yielded weighted mean age of 472.7 ± 10.4 Ma (2σ), suggesting that, if the leucogranite has an anatectic nature, partial melting of the metasedimentary supracrustal sequence was synchronous with the growth of intermediate plutonic bodies. The lack of age inheritance is the main reason why this leucogranite provides stronger evidence for the previous argument than those extracted from zircon ages in the metasedimentary rocks (see below).

Table 4. LA-MC-ICP-MS U-Pb Zircon Data for Tonalite VFKS11-4

	Concentration			Isotope Ratios						Apparent Ages (Ma)					
Spot	U (ppm)	Th (ppm)	Th/U	$^{206}Pbm/^{204}Pbc$	$^{207}Pb/^{235}U$	± SE (%)	$^{206}Pb/^{238}U$	± SE (%)	Error Correction	$^{206}Pb/^{238}U$	± SE (Ma)	$^{207}Pb/^{235}U$	± SE (Ma)	$^{206}Pb/^{207}Pb$	± SE (Ma)
1c	104	87	0.84	2065	1.36375	12	0.15297	8.1	0.65	917.6	69.1	873.5	72.7	763.3	198.4
1r	183	66	0.36	15072	0.59198	7	0.07337	1.7	0.25	456.4	7.5	472.1	25.8	549.2	144.8
2c	134	75	0.56	45135	2.08419	3	0.18817	1.5	0.43	1111.4	14.9	1143.6	23.5	1205.2	61.0
3c	134	147	1.10	13427	0.60898	10	0.07598	3.7	0.37	472.1	16.8	482.9	38.6	534.5	204.9
4c	172	264	1.53	657	0.58310	33	0.09615	3.0	0.09	591.8	17.1	466.4	124.7		
4	137	233	1.70	18066	0.77488	2	0.09244	1.4	0.76	569.9	7.6	582.6	8.1	632.1	25.7
5r	139	64	0.46	17867	0.64301	3	0.07820	1.9	0.72	485.4	8.8	504.2	10.4	590.5	39.6
6c	134	41	0.31	14565	0.68589	3	0.08451	2.3	0.68	523.0	11.7	530.3	14.0	561.9	53.9
6r	250	76	0.30	17194	0.58533	3	0.07427	2.1	0.67	461.8	9.6	467.9	12.0	497.7	52.4
7c	223	94	0.42	30093	0.60396	4	0.07403	2.9	0.69	460.4	12.8	479.7	16.0	573.4	65.8
8c	27	9	0.31	6959	1.87071	8	0.17592	6.8	0.88	1044.6	65.2	1070.8	50.8	1124.4	72.5
8c2	70	10	0.14	6343	1.78833	4	0.17435	2.7	0.72	1036.0	26.0	1041.2	24.6	1052.1	52.9
8r	237	63	0.27	20379	0.63789	4	0.07948	3.3	0.88	493.0	15.8	501.0	14.9	537.7	39.5
8r2	201	67	0.34	9236	0.61931	4	0.07854	4.0	0.96	487.4	18.7	489.4	16.1	498.9	25.7
9c	793	99	0.12	7223	0.83792	2	0.10038	1.0	0.56	616.7	5.9	618.0	8.2	622.9	31.6
9r	523	60	0.11	2429	0.78559	6	0.09271	4.0	0.68	571.5	21.8	588.7	26.2	655.3	92.3
10c	582	84	0.14	5597	1.03457	4	0.11852	3.3	0.78	722.1	22.4	721.2	21.8	718.6	56.4
11r	276	76	0.27	11878	0.58295	6	0.07397	3.4	0.60	460.0	14.9	466.4	21.0	497.6	99.1
12r	144	68	0.47	15941	0.65521	2	0.08090	1.4	0.70	501.5	7.0	511.7	8.3	557.4	32.3
13	240	127	0.53	22658	0.74962	1	0.09217	1.0	0.70	568.4	5.4	568.0	6.2	566.6	22.3
14r	166	92	0.55	4598	0.60860	4	0.07750	3.0	0.82	481.2	14.0	482.7	14.2	489.9	47.2
15r	221	111	0.50	12396	0.58719	2	0.07502	1.0	0.61	466.3	4.5	469.1	6.1	482.4	28.3
16c	168	81	0.48	19715	1.87956	2	0.18186	1.8	0.80	1077.1	18.0	1073.9	15.1	1067.3	27.4
16r	186	77	0.41	12255	0.62052	3	0.07859	3.0	0.92	487.7	14.0	490.2	12.7	501.9	28.7
17c	243	157	0.65	5360	0.63751	5	0.07890	3.6	0.76	489.5	17.1	500.8	18.7	552.4	66.6
18c	34	34	0.99	7483	1.94956	5	0.18281	2.8	0.52	1082.3	27.7	1098.3	35.5	1130.0	89.7
18r	153	60	0.39	14180	0.62088	3	0.07692	1.6	0.56	477.7	7.2	490.4	10.9	550.0	50.9
19c	187	105	0.56	9025	1.85466	2	0.17408	1.7	0.80	1034.5	16.4	1065.1	14.1	1128.2	25.3
19r	110	75	0.68	4762	0.62533	4	0.07751	3.2	0.86	481.3	15.1	493.2	14.7	548.9	42.0
20	76	136	1.80	260	0.48443	16	0.07438	2.3	0.15	462.5	10.4	401.1	52.9	61.0	378.3
21c	136	76	0.56	14898	1.72461	8	0.16779	7.0	0.88	999.9	64.6	1017.7	51.2	1056.3	77.4
21r	240	356	1.48	12313	0.69265	3	0.08565	1.8	0.58	529.8	9.1	534.4	12.8	554.2	55.0
22c	114	87	0.77	10438	1.43799	2	0.14953	1.5	0.78	898.3	12.7	904.9	11.6	920.9	25.1
22r	171	53	0.31	5988	0.61723	3	0.07748	1.0	0.37	481.1	4.6	488.1	10.5	521.3	55.0
23c	77	81	1.06	1992	0.69813	6	0.08414	2.5	0.38	520.8	12.3	537.7	27.1	609.9	129.9
23r	78	110	1.40	2645	0.62918	4	0.07916	2.0	0.53	491.1	9.5	495.6	15.0	516.3	71.4
24c	20	14	0.69	4481	2.12688	4	0.18228	2.1	0.57	1079.4	20.4	1157.6	25.0	1307.0	58.0
24r	82	66	0.81	4204	0.64729	3	0.07568	1.9	0.63	470.3	8.7	506.8	12.2	675.1	51.1
25c	76	52	0.68	8426	1.93149	2	0.18409	1.8	0.82	1089.3	18.2	1092.1	14.8	1097.6	25.5
25	137	78	0.57	17080	1.44400	4	0.14354	4.1	0.96	864.7	33.2	907.4	25.6	1012.8	23.8
26r	190	51	0.27	6431	0.61052	3	0.07714	1.9	0.64	479.0	8.8	483.9	11.6	506.9	50.9
27	195	88	0.45	14840	0.63595	3	0.07882	2.7	0.80	489.1	12.9	499.8	13.6	549.2	45.4
28	156	276	1.77	15055	0.62145	3	0.07727	2.7	0.86	479.8	12.5	490.8	12.2	542.3	35.2
29	153	99	0.65	8192	0.62236	4	0.07817	2.9	0.80	485.2	13.5	491.3	14.1	520.0	47.3

[44] An amphibole-bearing gabbro (VFKS10-5) from a tens of meters sized body was collected within the transitional intermediate unit (Figure 2). Zircons from this gabbro are characterized by Th/U ratios close to 1.0, and CL images show bright high-U wide rims (Figure 6b, inset). Twenty-three spot points were measured in zircons from this amphibole gabbro. The data set yielded a coherent group of 18 data with apparent concordance and no inheritance with a weighted mean age of 473.6 ± 3.9 Ma (Figure 6b). A subset of 5 data was rejected mainly because of high errors (>15%).

4.5. Granodiorites and Tonalite From the Silicic Unit

[45] Five granodiorites and one tonalite were collected in the silicic units (Figure 2). These samples are spread over a large area, ~15 km along strike so their distribution allows testing spatial U-Pb zircon age variations within the unit. Two granodiorites (VFKS11-2/4) were taken close to the contact between the intermediate transitional and the silicic units (Figure 2). In granodiorite VFKS11-2, 35 spot points were measures in zircons with both morphology and Th/U ratios typically of igneous systems (Figures 7a and 7b). The data set yielded a cluster of 22 spot points of concordant ages with a weighted mean age of 468.7 ± 8.4 Ma (Figure 9b). Ten spot points span a range of ages from paleo-Proterozoic to Middle Cambrian with a cluster of six data defining a $^{206}Pb/^{238}U$ age of 950 ± 50 Ma. Three additional points were rejected because of large discordance or high error (>15%).

[46] The other granodiorite (VFKS11-4) also shows the significance of the inheritance in this part of the silicic unit, as exactly one half of the data set from a total of 44 points

Table 5. LA-MC-ICP-MS U-Pb Zircon Data for Granodiorite VFKS12-6

	Concentration			Isotope Ratios						Apparent Ages (Ma)					
Spot	U (ppm)	Th (ppm)	Th/U	$^{206}Pbm/^{204}Pbc$	$^{207}Pb/^{204}Pbc$	± SE (%)	$^{206}Pb/^{238}U$	± SE (%)	Error Correction	$^{206}Pb/^{238}U$	± SE (Ma)	$^{207}Pb/^{235}U$	± SE (Ma)	$^{206}Pb/^{207}Pb$	± SE (Ma)
1r	171	35	0.20	3876	0.57498	7	0.07718	3.3	0.45563	479.3	15.2	461.2	26.8	372.3	144.8
1c	580	275	0.47	5884	0.59696	5	0.07541	2.7	0.48821	468.7	12.1	475.3	20.8	507.5	105.4
2r	611	678	1.11	886	0.51231	8	0.06996	3.5	0.41880	435.9	14.6	420.0	28.4	333.5	170.2
3c	109	77	0.70	2462	0.66487	9	0.08094	4.3	0.48669	501.7	20.7	517.6	35.7	588.2	166.9
4r	102	59	0.58	2256	0.58315	5	0.07551	3.1	0.58606	469.3	14.1	466.5	19.9	452.8	95.7
5r	562	466	0.83	8617	0.58014	5	0.07607	3.2	0.62314	472.6	14.5	464.6	19.1	424.8	89.3
6c	155	54	0.35	4048	0.62886	7	0.07678	3.1	0.42292	476.9	14.1	495.4	28.4	581.9	142.8
6t	816	133	0.16	8471	0.62506	3	0.07882	1.4	0.46581	489.1	6.8	493.0	12.1	511.3	60.3
7r	158	121	0.77	3699	0.61234	6	0.07908	4.9	0.81848	490.6	23.2	485.0	23.1	458.7	76.4
8c	387	116	0.30	3141	0.60076	4	0.07878	2.0	0.48750	488.9	9.5	477.7	15.7	424.5	80.4
9r	386	221	0.57	2300	0.56141	5	0.07524	2.8	0.56190	467.6	12.6	452.4	18.1	376.0	92.3
10r	178	42	0.23	3125	0.60340	6	0.07326	2.0	0.36700	455.8	9.0	479.4	21.3	594.0	112.2
11r	368	162	0.44	6885	0.58862	5	0.07518	2.6	0.54474	467.3	11.5	470.0	17.7	483.1	87.0
12r	483	216	0.45	8162	0.58356	3	0.07501	2.8	0.82057	466.3	12.7	466.7	12.9	469.1	43.7
13	860	426	0.50	9269	0.57031	4	0.07362	2.0	0.53317	457.9	8.9	458.2	14.0	459.7	71.3
14	549	238	0.43	5995	0.58914	5	0.07481	1.7	0.36790	465.0	7.6	470.3	17.4	496.1	94.8
15	691	422	0.61	11296	0.58960	3	0.07526	1.8	0.64684	467.7	8.3	470.6	10.7	484.6	47.9
16c	447	139	0.31	10179	0.61895	4	0.07512	1.1	0.28722	466.9	5.0	489.2	15.1	595.0	81.0
17c	592	257	0.43	17748	0.60584	3	0.07531	2.2	0.85418	468.0	10.1	480.9	10.0	542.8	29.7
18c	691	303	0.44	17114	0.60915	4	0.07591	1.7	0.46959	471.7	7.7	483.0	13.9	537.1	69.7
19	759	366	0.48	11236	0.59497	2	0.07616	1.5	0.59252	473.2	6.7	474.0	9.4	478.3	44.1
20	822	442	0.54	22299	0.61936	4	0.07785	2.9	0.69463	483.3	13.7	489.4	16.5	518.4	66.9
21	623	333	0.53	20198	0.59756	4	0.07453	2.5	0.66410	463.4	11.2	475.7	14.4	535.5	61.8
22	693	278	0.40	22351	0.60679	5	0.07700	2.8	0.54282	478.2	12.8	481.5	19.7	497.4	94.9

Table 6. LA-MC-ICP-MS U-Pb Zircon Data for Metasedimentary Migmatite VFKS09-1

	Concentration			Isotope Ratios						Apparent Ages (Ma)					
Spot	U (ppm)	Th (ppm)	Th/U	$^{206}Pbm/^{204}Pbc$	$^{207}Pb/^{235}U$	± SE (%)	$^{206}Pb/^{238}U$	± SE (%)	Error Correction	$^{206}Pb/^{238}U$	± SE (Ma)	$^{207}Pb/^{235}U$	± SE (Ma)	$^{206}Pb/^{207}Pb$	± SE (Ma)
1r	137	96	0.70	6382	0.72233	4	0.08888	3.2	0.86	548.9	16.6	552.0	15.7	565.1	41.1
2r	158	26	0.17	6189	0.61533	3	0.07662	2.1	0.77	475.9	9.8	486.9	10.7	539.0	38.3
3r	179	125	0.70	6864	0.69111	2	0.08553	1.3	0.55	529.0	6.4	533.5	9.6	552.4	42.3
4r	257	10	0.04	9062	0.60944	3	0.07684	1.2	0.41	477.2	5.6	483.2	11.6	511.7	60.5
5r	155	76	0.49	5943	0.70220	5	0.08550	2.9	0.57	528.9	14.6	540.1	21.1	587.8	89.8
6r	147	69	0.47	7068	0.79943	4	0.09511	1.0	0.23	585.7	5.6	596.5	19.5	637.8	90.3
7	115	151	1.32	7615	0.75039	4	0.09163	3.0	0.82	565.1	16.5	568.4	16.3	581.7	47.0
8c	70	57	0.82	2639	0.85799	5	0.09683	3.3	0.62	595.8	19.0	629.0	25.1	750.3	88.4
9	90	106	1.17	5258	1.00464	4	0.11701	3.6	0.85	713.3	24.2	706.2	21.4	683.4	46.8
10c	66	68	1.03	2621	0.88867	5	0.10850	1.0	0.20	664.0	6.3	645.7	24.5	581.9	109.1
11t	120	75	0.62	5700	0.77302	2	0.09492	1.7	0.70	584.6	9.5	581.5	10.8	569.5	38.0
12r	127	56	0.44	5683	0.80112	3	0.09552	2.2	0.67	588.1	12.4	597.5	14.8	633.1	52.1
13	402	192	0.48	15960	0.89161	4	0.10529	2.6	0.62	645.4	15.9	647.2	20.0	653.8	70.1
14c	104	35	0.33	32668	13.48956	3	0.52715	1.8	0.71	2729.4	40.7	2714.6	24.5	2703.5	30.2
15r	60	20	0.34	3526	1.08823	4	0.11589	2.4	0.65	706.9	15.9	747.6	19.3	871.7	57.4
16	99	36	0.36	3418	0.78524	6	0.09444	5.4	0.86	581.7	29.8	588.5	27.7	614.6	67.7
17r	153	36	0.23	7116	0.70549	5	0.08595	2.2	0.41	531.5	11.4	542.1	23.0	586.6	108.7
18r	490	446	0.91	14154	0.72209	4	0.08866	3.2	0.73	547.6	16.7	551.9	18.4	569.5	64.1
19	154	170	1.10	7281	0.83254	4	0.09622	2.2	0.53	592.2	12.5	615.0	19.2	699.8	75.3
20r	205	104	0.51	7347	1.01435	3	0.11725	1.0	0.33	714.7	6.8	711.1	15.5	699.6	61.1
21c	221	91	0.41	11912	1.47656	2	0.15193	1.0	0.47	911.7	8.7	920.8	13.2	942.6	39.3
22r	182	266	1.46	5926	0.73905	7	0.09067	5.4	0.81	559.5	29.2	561.9	29.0	571.3	85.8
23c	207	115	0.56	6531	1.50747	6	0.15477	2.0	0.33	927.6	17.7	933.4	37.6	947.1	119.0
24c	124	88	0.71	4287	0.80357	2	0.09736	1.7	0.70	598.9	9.7	598.8	11.0	598.5	38.0
24r	144	69	0.48	4355	0.78708	3	0.09670	2.2	0.69	595.1	12.5	589.5	14.4	568.2	51.1
25r	106	49	0.46	1957	0.91507	10	0.10370	3.3	0.32	636.1	19.8	659.8	49.4	741.6	204.1
26r	140	112	0.80	4526	0.67995	3	0.08443	2.5	0.74	522.5	12.4	526.7	13.6	545.2	48.6
27c	84	69	0.81	4761	2.01318	4	0.18747	1.0	0.28	1107.7	10.2	1120.0	23.8	1143.9	66.9
28r	314	176	0.56	5534	0.77353	4	0.09506	1.8	0.43	585.4	10.1	581.8	18.4	567.6	81.7
29r	128	71	0.55	3822	1.13035	8	0.12790	4.4	0.56	775.9	32.5	767.9	42.7	744.8	139.0
30c	98	48	0.49	2362	0.74575	9	0.09065	4.0	0.47	559.4	21.3	565.8	37.1	591.5	164.0

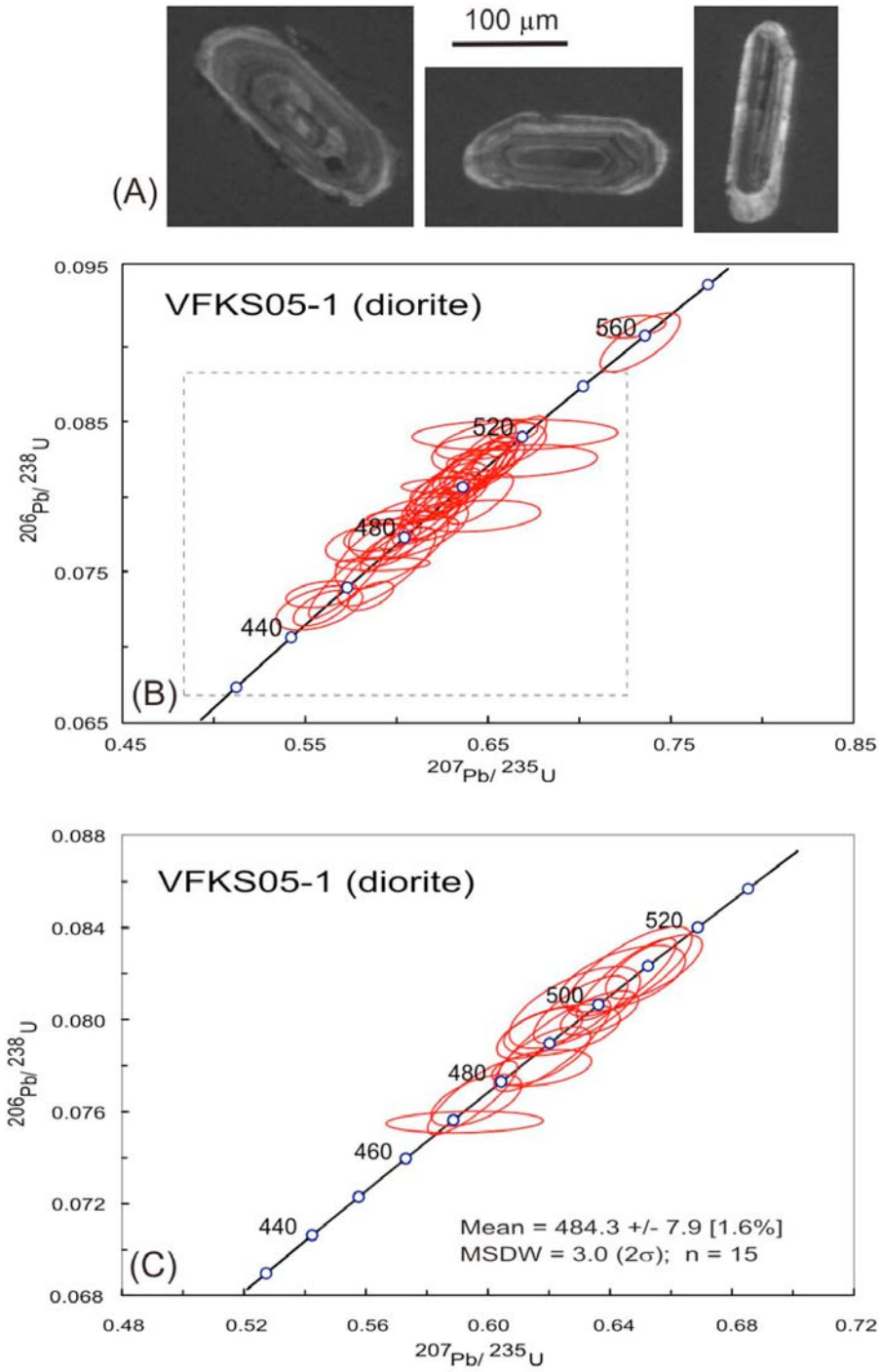

Figure 3. Conventional concordia diagrams zircons from the upper part of the mafic unit (sample VFKS05-1). Errors are shown as ellipses at the 2σ level. All results are represented graphically using ISOPLOT [*Ludwig*, 2003]. (a) Cathodoluminescence images of representative zircon crystals showing prismatic shapes and internal oscillatory zoning. (b) Concordia diagram showing the Pb/U data of all analyzed zircons. (c) Same as Figure 3b but displaying spot used to calculate the weighted age. Note that the dashed box in Figure 3b outlines the area of Figure 3c.

yielded inherited core ages older than 500 Ma, which is the oldest Famatinian magmatic age [e.g., *Pankhurst et al.*, 2000]. Furthermore, four clusters of inherited ages define peaks at 569, 617, 901, and 1120 Ma (Figure 7c). The largest cluster (n = 13) of concordant points constrain the Ordovician crystallization age of the sample, which has a mean age of 481.5 ± 7.9 Ma. Seven spots were excluded due to discordance. It is possible that the laser beam (which

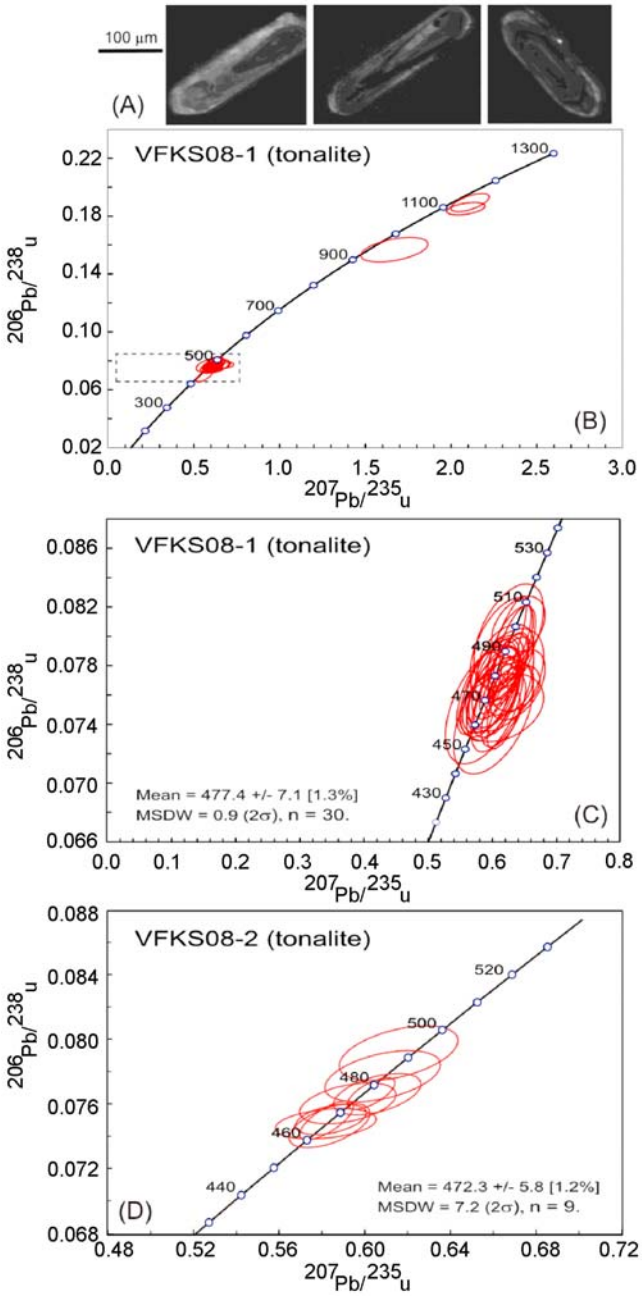

Figure 4. Concordia diagrams for zircons from the intermediate unit. Errors are shown as ellipses at the 2σ level. (a) Cathodoluminescence images of representative zircon crystals from tonalites showing long prismatic shapes and internal oscillatory zoning (sample VFKS05-1). (b) Concordia diagram showing the Pb/U data of all analyzed zircons from specimen tonalite VFKS08-1. (c) Same as Figure 4b but displaying spot used to calculate the weighted age for this tonalite. The dashed box in Figure 4b outlines the area of the diagram in Figure 4c. (d) Concordia diagram showing the Pb/U spot point used to calculate the weighted age for tonalite VFKS08-2.

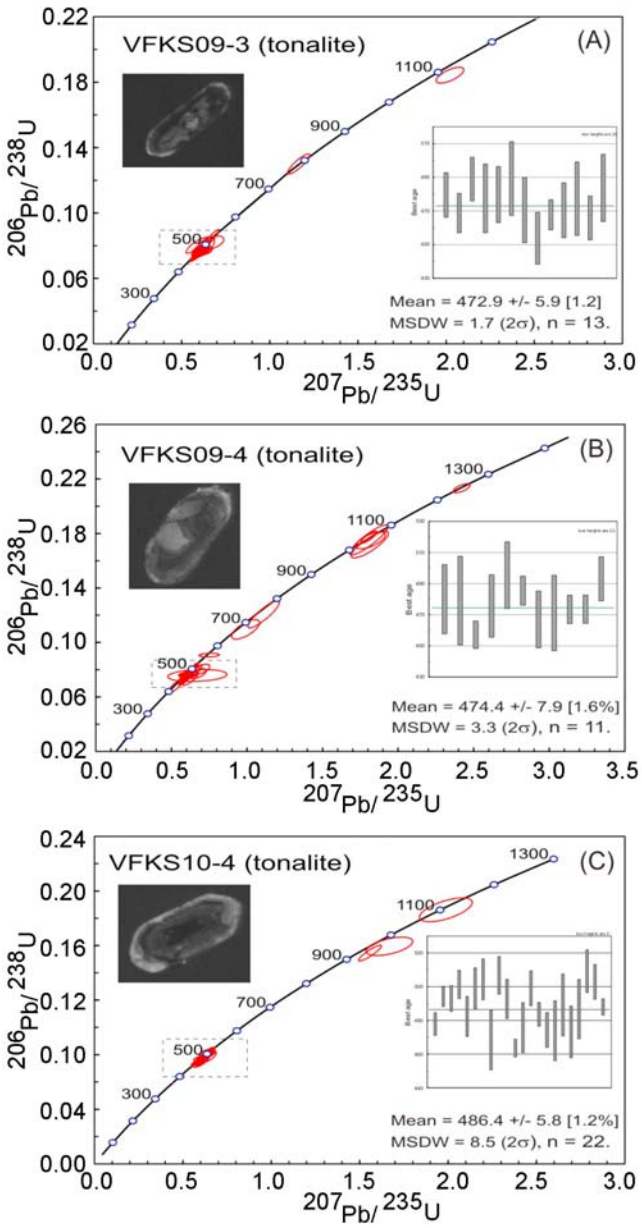

Figure 5. Concordia diagrams for zircons from the transitional unit between intermediate and silicic units. Errors are shown as ellipses at the 2σ level. (a, b, and c) For the three tonalitic samples taken from this unit and showing the Pb/U data of all analyzed zircons from each specimen. Spot points used to extract the weighted crystallization ages fall within the area outlined by the dashed box. Insets show $^{206}Pb/^{238}U$ ages of those stop points used to extract the weighted mean age, and error bars show the standard deviation (expressed at 2σ level) for each spot age. Cathodoluminescence images of typical zircon crystals from each tonalite are also shown as an inset; note the existence of stubby cores that in some cases yielded inherited ages.

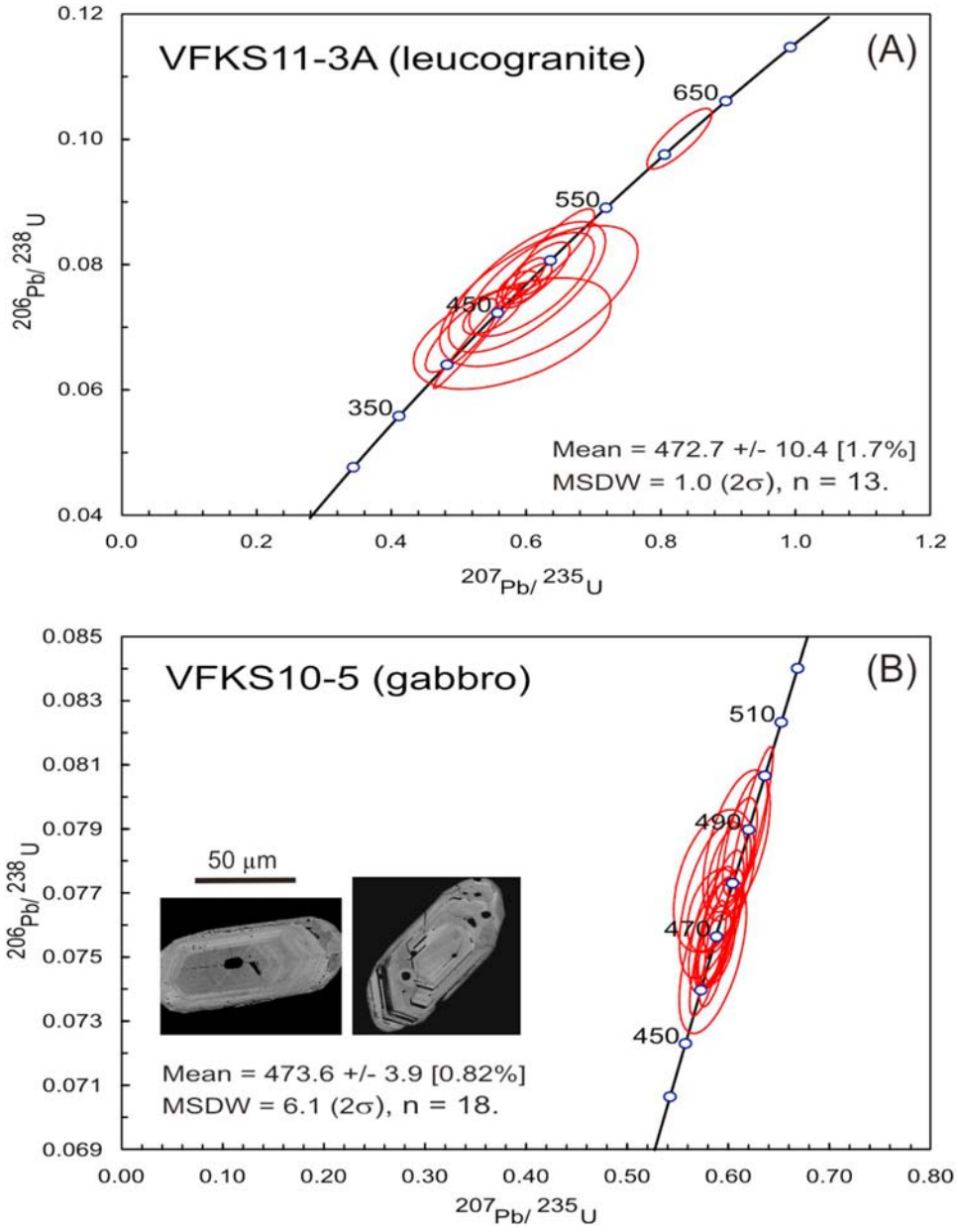

Figure 6. Concordia diagrams for zircons from (a) a leucogranite and (b) a gabbro included as subordinate lithologies in the transitional unit. Errors are shown as ellipses at the 2σ level. Cathodoluminescence images of typical zircon crystals from the gabbroic rock are also shown as inset in Figure 6b.

cannot be routinely focused to <25 μm in diameter with the analytical setup used in this study) hitting slightly older domains influences the older pooled age.

[47] Granodiorite VFKS11-5A was collected from the eastern end of the east–west section (Figure 2). In contrast with the majority of the samples from the silicic unit, this granodiorite lacks inherited ages. Only one out of 22 measured grains with apparent concordance of 512 Ma has an age older than 500 Ma. There is a cluster (n = 14) of data with a weighted average on $^{206}Pb/^{238}U$ ages of 470.3 ± 7.7 Ma (Figure 7d). Rejection of seven analyses from zircon grains was made on the basis of large discordance or high error (>15%).

[48] Thirty-one zircon spot points were determined in a tonalite (VFKS12-2) that is magmatically commingled with the granodiorites from the silicic unit (Figure 2). Zircon points of this tonalite yielded a coherent group of 25 $^{206}Pb/^{238}U$ and $^{207}Pb/^{235}U$ ratios with apparent concordance and a weighted mean $^{206}Pb/^{238}U$ age of 492.2 ± 6.8 Ma (Figure 8a). However, the 25 spot points show spread of concordant ages spanning around 50 Ma from 516 to 462 Ma, leading to an age distribution too broad to be interpreted as a

statistical dispersion of a single age. Two additional inherited cores yielded best ages of 756 Ma and 2576 Ma. Only one point was rejected because of its strong deviation from the coherent group.

[49] Three granodiorites (VFKS12-4, VFKS12-6, and VFKS12-8A) were collected 8 km to the north of the main transect within the silicic unit (Figure 2). Thirty-one spots points were measured in 20 zircons from specimen VFKS12-4. This data set yields a coherent group of 25 points with apparent concordance, no inheritance, and with a weighted mean age of 476.4 ± 9.8 Ma (Figure 8b). Three data from inherited cores yielded $^{206}Pb/^{238}U$ ages within the Neoproterozoic. Three points were rejected due to strong deviation from the coherent group or high error.

[50] Since the weighted average of 20 spots on $^{206}Pb/^{238}U$ ages is 469.6 ± 2.3 Ma with MSWD < 1, the cluster of ages from granodiorite (VFKS12-6) is one of the most consistent and reliable (Figure 8c). Although seven spot points were rejected (Table 5), this granodiorite is unique in giving a tight range of ages and not having any inherited core.

[51] Twenty-nine zircon points were analyzed from granodiorite (VFKS12-8A) yielding a coherent group of 21 with apparent concordance and with a weighted mean age of 473.4 ± 8.2 Ma (Figure 8d). Five inherited zircon cores gave best ages from Archean to Early Cambrian (not shown). Three analyses from zircon grains were rejected on the basis of large errors (>15%).

4.6. Metapelitic Migmatitic Septum Within the Intermediate Unit

[52] This metapelitic migmatite (VFKS09-1) was taken from a thick septum that is surrounded by tonalites from the intermediate unit (Figure 2). The migmatite has in terms of shape, size and color a somewhat uniform population of zircon grains. However, the habit and internal features of the zircons from the metasedimentary migmatite are clearly distinct from those that are characteristic of the igneous plutonic lithologies. In general, zircon grains are slightly resorbed and inclusion-free (Figure 9a, insets). Under cathodoluminescence imaging, most of these zircons have a dark irregular core and show zoning consisting of few wide bands with brightness increasing toward their rims. There are also few anhedral unzoned grains (Figure 9a).

[53] The data set for the metapelitic migmatite includes 31 spot points measured in 19 zircon grains (Table 6). Importantly, there are several clusters of inherited core ages defining peaks at 531, 585 and 913 Ma (Figure 9b). Furthermore, two single data gave Mesoproterozoic and Late Archean best ages (Figure 9c). The largest coherent group of

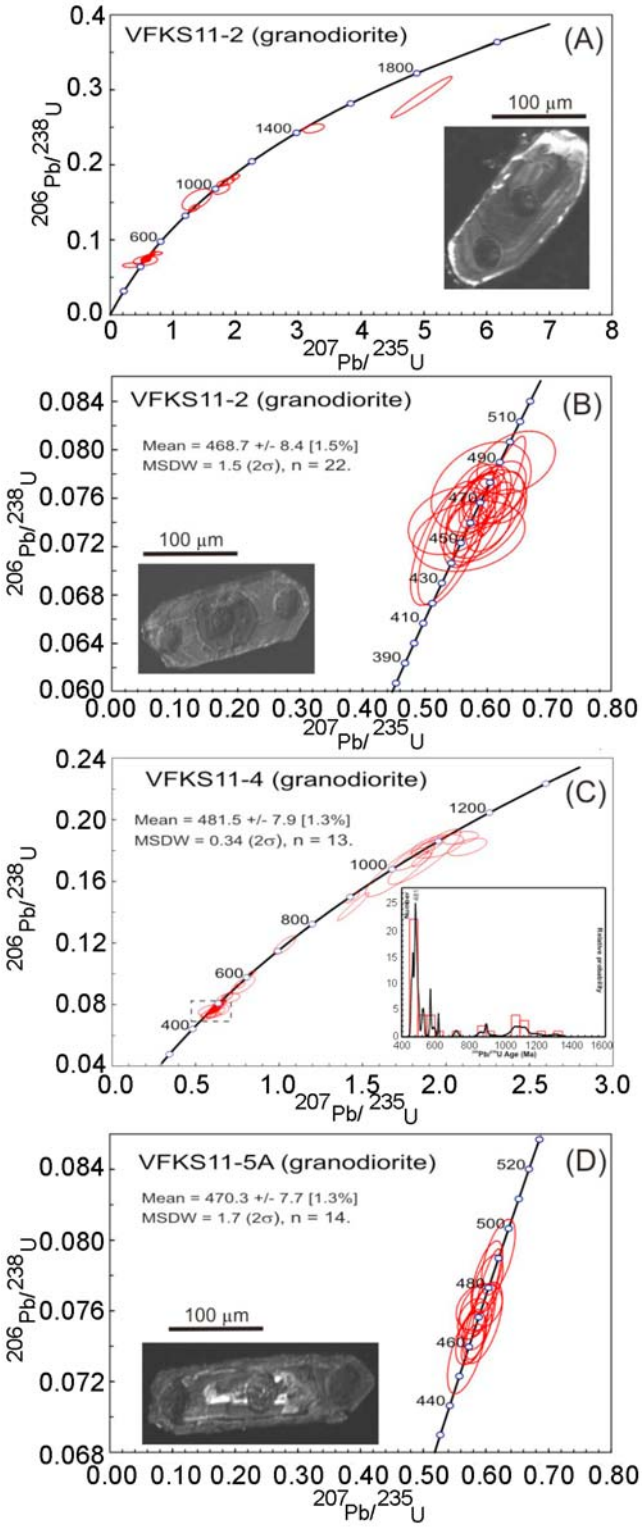

Figure 7. Concordia diagrams for zircons from the silicic unit. Errors are shown as ellipses at the 2σ level. (a) Concordia diagram that shows the Pb/U data of all analyzed spot points in granodiorite VFKS11-2. (b) Same as Figure 7a but displaying spot used to calculate the weighted age for this granodiorite. (c) Concordia diagram that shows the Pb/U data of all analyzed spot point in granodiorite VFKS11-4. The cumulative probability of $^{206}Pb/^{238}U$ ages for sample VFKS11-4 is shown in the inset; the probability diagram shows the age peaks of inherited zircon cores. (d) Concordia diagram showing the Pb/U spot points used to calculate the weighted age for granodiorite VFKS11-5A. Cathodoluminescence images of typical zircon crystals from the granodiorites are also shown as insets; note that laser pits (25 μm diameter) are visible in these zircons.

$^{206}Pb/^{238}U$ zircon ages is defined by 12 points with a weighted mean of 585.4 ± 7.7 Ma (Figure 9c). In terms of statistical significance the second most important cluster (n = 5) gave a Lower Cambrian age (531 Ma). Following these two clusters, two rims of zircon grains yielded an ages of 476.9 ± 11.4 Ma. The later age is consistent with zircon rim ages measured in other metasedimentary migmatites from the Sierra Valle Fértil [e.g., *Rapela et al.*, 2001], and regarded as caused by arc magmatism-related metamorphism [*Rapela et al.*, 2001; *Otamendi et al.*, 2008]. Neoproterozoic and Lower Cambrian age peaks will be further discussed below.

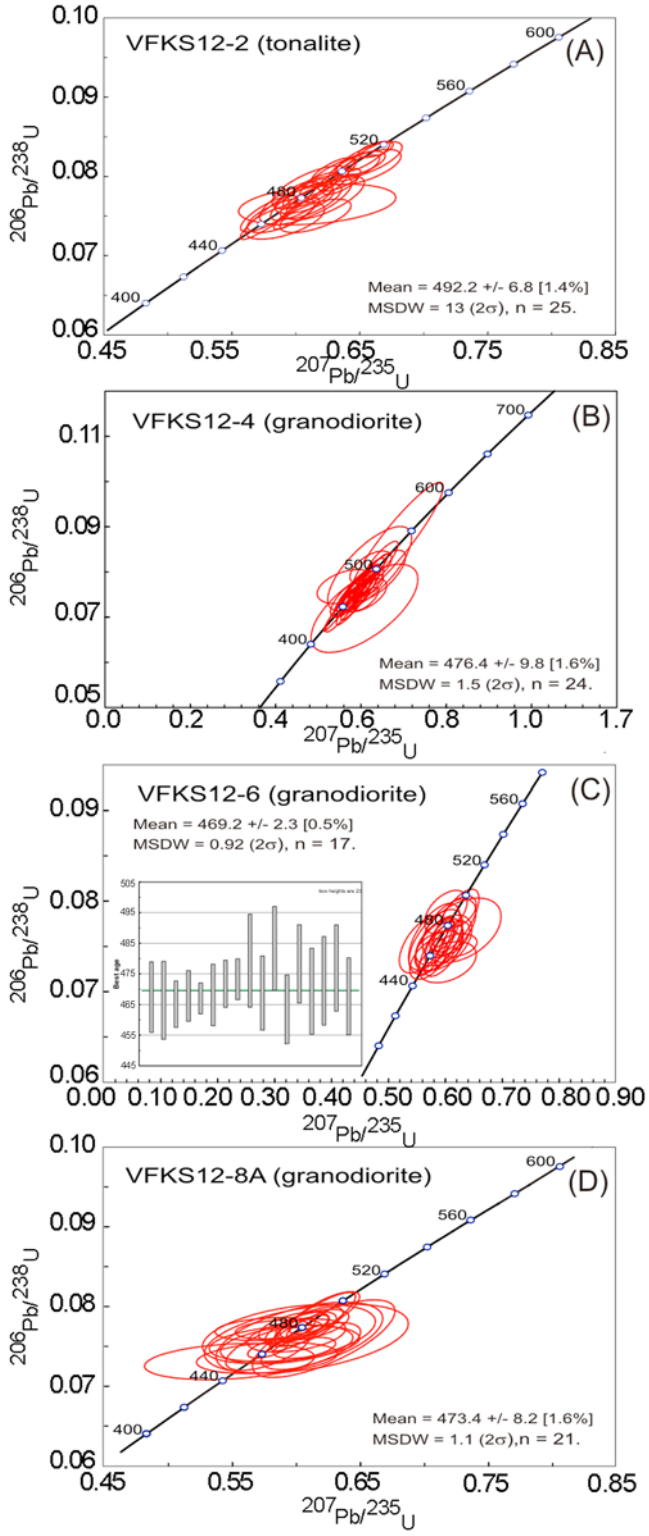

Figure 8. Concordia diagrams for LA-MC-ICP-MS analyses of zircons from the silicic unit. Errors are shown as ellipses at the 2σ level. (a) Concordia diagram showing the Pb/U spot points used to calculate the weighted age for tonalite VFKS12-2. (b) Concordia diagram showing the Pb/U spot points used to calculate the weighted age for granodiorite VFKS12-4. (c) Concordia diagram showing the Pb/U spot points used to calculate the weighted age for granodiorite VFKS12-6. Inset shows the $^{206}Pb/^{238}U$ ages of 17 points with error bars of the standard deviation expressed at 2σ level. (d) Concordia diagram showing the Pb/U spot point used to calculate the weighted age for granodiorite VFKS12-8A.

5. Discussion

5.1. Age of Arc Emplacement

[54] The crystallization age range for magmatic samples presented above is within the range of previously published regional geochonologic results on Famatinian arc plutonic rocks. Moreover, it appears that the bulk of magmatism building the arc in the Sierra Valle Fértil section took place over about ~20 Myr, from 465 to 485 Ma. Eleven out of 15 samples of igneous rocks yielded ages between 469 to 477 Ma (see Table 7) and given the size of errors reported in this study and elsewhere, it is possible that the arc construction took place over a much shorter time, as little as 5 Myr.

[55] Magmatic production in ~20 Myr high-flux events separated by lulls is common in Cordilleran arcs [*Ducea and Barton*, 2007; *DeCelles et al.*, 2009]. The emplacement of mafic magmas in the section was coeval with the felsic batholith generation, as evidenced by data presented in this paper. In order to calculate magmatic fluxes as "magmatic addition rates" in $km^3\ km^{-1}\ Myr^{-1}$ [*Reymer and Schubert*, 1984], the arc width is needed in addition to estimates of thicknesses of various magmatic rocks and timing information. We assume an arc width of 100 km, which is reasonable based on our general knowledge of Cordilleran magmatic arcs elsewhere, and also consistent with palinspastic reconstructions of the Famatinian arc (our work in progress). We estimate a minimum magmatic addition rate of ~30 $km^3\ km^{-1}\ Myr^{-1}$ from the mantle during the 20 Ma flare-up, assuming an average 6 km thickness of mafic rocks added to the crust over 20 Ma and a felsic/mafic ratio of ~3.5 in this crustal section, based on the map distribution of felsic plutonic rocks (Figure 2). Felsic plutons here are somewhat arbitrarily considered rocks that have >55% SiO_2, whereas mafic rocks are those that contain <55% SiO_2. The felsic plutons contain on average about 20–30% mixed mafic material in them, as documented by elemental and

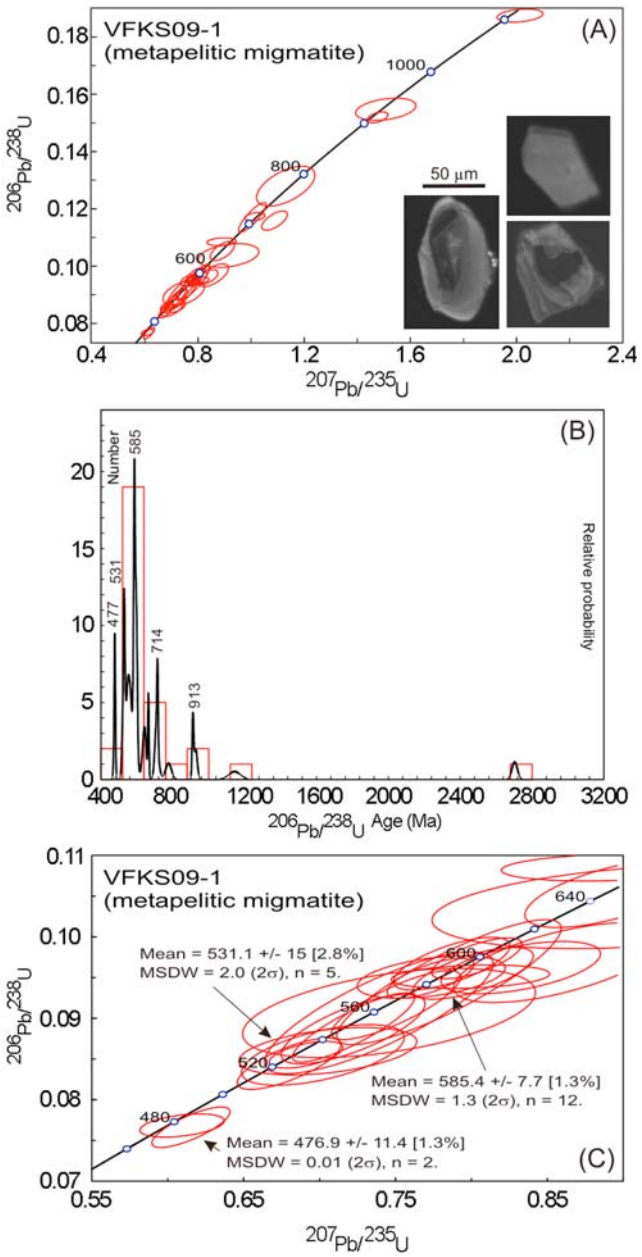

Figure 9. Concordia diagrams zircons from a metapelitic septum in the intermediate unit. Errors are shown as ellipses at the 2σ level. (a) Concordia diagram that shows the Pb/U data of all analyzed spot points in metapelitic migmatite VFKS09-1. Cathodoluminescence images of typical zircon crystals from the metapelite are shown as insets. (b) Cumulative probability of $^{206}Pb/^{238}U$ ages for sample VFKS09-1. (c) Concordia diagram with spot points pooled from the metapelite yielding ages that are (sub)concordant and lower than 640 Ma.

isotopic modeling [*Otamendi et al.*, 2009a], so the actual mafic to felsic ratio is slightly higher. However, these data show that felsic batholiths can be generated at high flux rates of over 100 km^3 km^{-1} Myr^{-1} in incipient arcs, similar to major high-flux events reported in mature continental arcs [*Ducea and Barton*, 2007]. These estimates for the Famatinian arc are minimum values as the life of the arc-related crustal construction may be as much as 4 times shorter, given the above mentioned uncertainties in age data. A similar high-flux event has been recently reported for the Jurassic intermediate arc of the Coast Mountains batholith in British Columbia, also an incipient continental arc [*Gehrels et al.*, 2009]. Other early stage high-flux events like the Jurassic one in the Sierra Nevada batholith [*Ducea*, 2001] are partly obscured by subsequent high-flux events, most likely by reworking of older arc material in younger plutons.

[56] The migmatite sample has pre-Ordovician (detrital?) zircons and a few metamorphic zircons that grew during the magmatic flare-up (465–485 Ma). On the basis of field evidence and these ages, we interpret that the parental metasedimentary rock of the migmatite underwent high-temperature metamorphism and partial melting synchronous with the Ordovician magmatism, a conclusion similar to that of *Rapela et al.* [2001]. The results are relevant as they show that the Famatinian magmatic arc at Sierra Valle Fértil lasted about 20 Ma, and terminated just when the accretion of Precordilleran terrane on western Gondwana margin began (circa 465–460 Ma [*Thomas and Astini*, 1996]).

5.2. Implications for Continental Arc Magmatism

[57] The Famatinian arc was clearly a continental one as it straddles the western margin of Gondwana in the modern coordinates of South America. There is no evidence that the South American cratonic basement crust was involved in magmatism in the Sierra Valle Fértil region; instead, the arc was emplaced exclusively into an extensive upper crustal sedimentary assemblage that most likely constitutes the accumulation of submarine passive margin sediments along Gondwana's margin during the Neoproterozoic and early Paleozoic prior to subduction. However, all gabbros that have been analyzed in this section have radiogenic isotopic characteristics typical of old (Precambrian) continental lithosphere [*Otamendi et al.*, 2009a], suggesting that South American lithosphere, perhaps thinned at a miogeoclinal margin, was in fact the framework of this arc. There is also no evidence that the crust became unusually thick during the Famatinian arc magmatism, as no rocks deeper than ~25–30 km are exposed at the surface to the west of the studied area based on our preliminary field observations and mapping of index minerals within metamorphic framework rocks, or elsewhere within the exposed plutonic framework of the Famatinian arc in central South America. In addition, there is also no evidence for crustal magmas (felsic plutons or volcanics) that derived from thicker parts of the crust (J. E. Otamendi et al., manuscript in preparation, 2010). No shortening or extension disrupted the architecture of the section studied here during the arc formation. Instead, the arc developed statically as a series of sills progressively emplaced into the existing crust, similar to the early stages (Jurassic) of Cordilleran magmatism in North America and to Cordilleran interior arcs that developed in North America during periods of shallow subduction as magmatism migrated inland [*Barton*, 1996].

Table 7. Summary of Age Records of Rocks From the Central Sierra Valle Fértil

Sample	Rock Type	Ordovician	Inherited
VFKS05-1	Diorite	span from 510 to 470 Ma (n = 15)	circa 560 Ma
VFKS08-1	Tonalite	477.4 ± 7.1 (2σ, n = 30)	span from 1127 to 1238 Ma
VFKS08-2	Tonalite	472.3 ± 5.8 Ma (2σ, n = 9)	
VFKS09-1	Migmatite	476.9 ± 11.4 Ma (2σ, n = 2)	585.4 ± 7.7 Ma (n = 12), peaks at 531 and 913 Ma.
VFKS09-3	Tonalite	472.9 ± 5.9 Ma (2σ, n = 13)	
VFKS09-4	Tonalite	474.4 ± 7.9 Ma (2σ, n = 11)	four ages at 1054 ± 46.4 Ma (2σ)
VFKS10-3A	Leucogranite	472.7 ± 10.4 Ma (2σ, n = 13)	
VFKS10-4	Tonalite	486.4 ± 5.8 Ma (2σ, n = 22)	span from 950 to 1100 Ma
VFKS10-5	Gabbro	473.6 ± 3.9 Ma (2σ, n = 18)	
VFKS11-2	Granodiorite	468.7 ± 8.4 Ma (2σ, n = 35)	six ages at 950 ± 50 Ma
VFKS11-4	Tonalite	481.5 ± 7.9 Ma (2σ, n = 13)	cluster peaks at 569, 617, 901, and 1120 Ma
VFKS11-5A	Granodiorite	470.3 ± 7.7 Ma (2σ, n = 14)	
VFKS12-2	Tonalite	span from 462 to 516 Ma (n = 25)	
VFKS12-4	Granodiorite	476.4 ± 9.8 Ma (2σ, n = 25)	three ages at Neoproterozoic
VFKS12-6	Granodiorite	469.6 ± 2.3 Ma (2σ, n = 20)	
VFKS12-8A	Granodiorite	473.4 ± 8.2 Ma (2σ, n = 21)	five ages span from late Achaean to early Cambrian

[58] We show that magmatic input from the mantle at an average rate of mafic arc magmatism worldwide [*Reymer and Schubert*, 1984] can provide enough heat and mass available for mixing with a preexisting metamorphic basement to generate a batholith scale crustal section within a short period of time, some 20 Myr or less. The architecture of the arc is one of multiple tens to hundreds of meter thick amphibole-rich gabbroic sills injected into a midcrustal section, where they mix with partial melts derived from a metasedimentary framework. All mantle-derived melts intruded in the section are wet gabbros and magmatic fractionation trends observable through field relationships suggest that some of these bodies transition to mafic diorites in their upper parts via closed system fractionation. There is no evidence that gabbros in this section fractionated to intermediate (higher silica) rocks, nor is there evidence that they ever remelted to generate more felsic melts. A signature feature of the entire Sierra Valle Fértil area is that virtually every outcrop in which we observe transitions from the mafic to tonalitic/granodioritic rocks is in close vicinity to a metasedimentary pendant or contains "ghosts" of it (identifiable rock enclaves, areas rich in cordierite and almandine garnet) within the more felsic units. Thus we use our extensive field observations at the scale of this study and a moderate knowledge of the entire range to emphatically state that with the exception of local closed system fractionation to mafic diorite of gabbroic sills, the entire compositional diversity of the Famatinian batholith, which includes the full compositional spectrum of Cordilleran calc-alkaline suites such as quartz-diorites, monzonites, tonalities, granodiorites, and granites, is generated by various hybridization processes between mantle-derived gabbros and diorites and the Puncoviscana metasedimentary rocks and their high-grade equivalents [*Otamendi et al.*, 2009a, 2009b].

[59] We suggest that any incipient arc developed on a continental upper plate in a subduction system may have similar characteristics to the Sierra Valle Fértil section. They are static arcs emplaced as a series of mafic sills that ignite melting of and mixing with their framework rocks at magmatic rates that can be higher than 100 km^3 km^{-1} Myr^{-1}, depending on how melt fertile the framework is. The Jurassic arcs of North American Cordillera may have been equivalents to the Famatinian arc. In addition, island arcs emplaced into crust that experienced long-lived subduction and have sizable trench and fore-arc accumulations (like modern Japan, the Caribbean, and parts of the Aleutians where the upper plate is continental) may have similar crustal architectures.

5.3. Geological Significance of Zircon Age Inheritance

[60] Within both plutonic and metasedimentary rocks from the Sierra Valle Fértil, inherited zircon cores reveal the detritus of several early magmatic events and cover the spectrum from late Archean to early Paleozoic orogenic cycles (Figures 5–9). The inherited core zircon ages for all of the rocks from the Sierra Valle Fértil define mainly late Mesoproterozoic–early Neoproterozoic (circa 1150–850 Ma) and Neoproterozoic–early Cambrian (circa 720–530 Ma) populations, reflecting zircon inheritance from Grenvillian-type, Brasiliano–Pan African and Pampeano orogenic cycles (as defined and used by, e.g., *de Brito Neves and Cordani* [1991], *Trompette* [1997], *Rapela et al.* [1998, 2007], and *Cordani et al.* [2010]).

[61] The relative proportions of inherited zircons vary for the distinct major rock types. Plutonic tonalites and granodiorites have inherited zircon pattern with cluster of ages around 1050 Ma, reflecting a well-preserved Grenvillian age (~1 Ga) inheritance. The zircon population with late Neoproterozoic–early Cambrian (>520 Ma) ages appears subordinate in the intermediate and silicic plutonic rocks. By contrast, zircon inheritance patterns of the metasedimentary migmatite shows two peaks at around 585 Ma and 535 Ma (Figures 9a and 9b).

[62] In central western Argentina, detrital zircons of these ages are characteristic of thick sedimentary sequences with depositional ages that spread over the late Neoproterozoic and early Cambrian [*Schwartz et al.*, 2004; *Adams et al.*,

2008; *Steenken et al.*, 2006; *Rapela et al.*, 2007]. In effect, dating of detrital zircon has proved to provide one of the strongest evidence that the sedimentary sequences were eastwardly sourced in the South American continental interior and filled a large basin known as Puncoviscana through [e.g., *Ježek et al.*, 1985]. Detrital zircons from the Puncoviscana Formation yielded two distinctive population maxima at 1150–850 Ma and 650–520 Ma [e.g., *Adams et al.*, 2008] that are broadly similar to those found in sedimentary packages metamorphosed during the early Cambrian Pampean cycle and early Ordovician Famatinian magmatic arc [*Schwartz et al.*, 2004; *Steenken et al.*, 2006; *Rapela et al.*, 2007; *Drobe et al.*, 2009].

[63] Most studies have interpreted the sources of the late Mesoproterozoic, Neoproterozoic and early Cambrian zircons to be Gondwanan. This is because detrital zircons were derived from orogenic systems generated during successive amalgamation of cratonic landmasses of South America and the once contiguous cratons of southwestern Africa [*Rapela et al.*, 1998, 2007; *Schwartz et al.*, 2004; *Adams et al.*, 2008]. Although there is still strong discrepancy about the exact tectonic setting (i.e., passive versus active continental crustal margin) the prevalent model is that Puncoviscana and equivalent sedimentary sequences deposited in a large basin evolving along the margin of western Gondwana [*Ježek et al.*, 1985; *Zimmermann*, 2005; *Rapela et al.*, 2007; *Drobe et al.*, 2009]. By implication, the Ordovician tonalitic and granodioritic plutonism were built up into supracrustal sedimentary sequence that filled basins at the outboard of a western Gondwanan landmass. Since the lower mafic crust of the Famatinian arc is below the tonalitic intermediate unit and there is isotopic evidence for a cratonic basement underlying the supracrustal packages, the exact origin of Puncoviscana basin remains open to question.

6. Conclusions

[64] New age data for the emplacement of the Famatinian arc show that the arc was built during a period of ~20 Myr (from 485 Ma to 465 Ma) with a mantle-derived mafic flux typical of island arcs (~30 km^3 km^{-1} Myr^{-1}) and that intermediate to felsic calc-alkaline magmas formed synchronously via extensive melting of a supracrustal component and mixing with gabbros and (possibly) minor amounts of diorites fluxed from the mantle. The rate of felsic magma generation was about three times higher than the mafic flux, similar to flare-up events in other Cordilleran batholiths. This rate could not have continued for felsic magmatism without additional crustal mass added to the upper plate, as most of the existing metasedimentary framework had been depleted of its fusible components. This study adds to an increasing number of observations that suggest a nonsteady state behavior of intermediate arc magmatism along continental margins, and shows that static arcs, such as those formed along incipient subduction or in more mature arcs within cordilleran interiors can produce batholith-sized magmatic accumulations in short periods of time, <20 Myr in this case. The total volume of intermediate to silicic magmatism generated by the Famatinian arc regionally is difficult to estimate due to lack of complete sections, as well as the severe disaggregation of the arc following its Ordovician buildup, but exposures of similar rocks (age, composition) over an area exceeding 1500 km along the strike of the central Andes make it clear that the Famatinian arc generated in the range of 1×10^6 km^3 or more of felsic magmatism, similar to the younger large batholiths of western North America.

[65] The Sierra Valle Fértil arc section provides great insights into the evolution of the "early" stages of Cordilleran arcs, before they experience major crustal thickening and crustal overturn in the upper plate, and is especially important because of the existence of a comprehensive, perhaps unparalleled record of wet mafic magmas archived in its lower crustal exposures. We suggest the Famatinian arc section is an equivalent to the crustal architecture of more mature modern island arcs, such as parts of the Caribbean and Japan.

[66] **Acknowledgments.** This research was partly support by a COSA Exxon-Mobil grant to Mihai Ducea and University of Arizona colleagues and a FONCYT-Argentinian grant to Juan Otamendi. We thank Associate Editor Margi Rusmore and two anonymous reviewers for greatly improving the manuscript through constructive comments and suggestions.

References

Aceñolaza, G. F. (2003), The Cambrian system in northwestern Argentina: Stratigraphical and palaeontological framework, *Geol. Acta*, *1*, 23–29.

Aceñolaza, G. F., H. Miller, and A. J. Toselli (2000), The Pampean and Famatinian cycles: Superposed orogenic events in West Gondwana, *Z. Angew. Geol.*, *SH1*, 337–344.

Adams, C. J., H. Miller, A. J. Toselli, and W. L. Griffin (2008), The Puncoviscana Formation of northwest Argentina: U-Pb geochronology of detrital zircons and Rb-Sr metamorphic ages and their bearing on its stratigraphic age, sediment provenance and tectonic setting, *Neues Jahrb. Geol. Palaeontol. Abh.*, *247*, 341–352, doi:10.1127/0077-7749/2008/0247-0341.

Armstrong, R. L. (1988), Mesozoic and early Cenozoic magmatic evolution of the Canadian Cordillera, in *Processes in Continental Lithospheric Deformation*, edited by S. P. Clark Jr., B. C. Burchfiel, and J. Suppe, *Spec. Pap. Geol. Soc. Am.*, *218*, 55–91.

Astini, R. A., and F. M. Dávila (2004), Ordovician back arc foreland and Ocloyic thrust belt development on the western Gondwana margin as a response to Precodillera terrane accretion, *Tectonics*, *23*, TC4008, doi:10.1029/2003TC001620.

Babeyko, A. Y., S. V. Sobolev, and R. B. Trumbull (2002), Numerical models of crustal scale convection and partial melting beneath the Altiplano-Puna plateau, *Earth Planet. Sci. Lett.*, *199*, 373–388, doi:10.1016/S0012-821X(02)00597-6.

Barazangi, M., and B. I. Isacks (1976), Spatial distribution of earthquakes and subduction of the Nazca plate beneath South America, *Geology*, *4*, 686–692, doi:10.1130/0091-7613(1976)4<686:SDOEAS>2.0.CO;2.

Barton, M. D. (1996), Granitic magmatism and metallogeny of southwestern North America, *Trans. R. Soc. Edinburgh Earth Sci.*, *87*, 261–280.

Beard, J. S. (2008), Crystal-melt separation and the development of isotopic heterogeneities in hybrid magmas, *J. Petrol.*, *49*, 1027–1041, doi:10.1093/petrology/egn015.

Calvert, A. J., S. L. Klemperer, N. Takahashi, and B. C. Kerr (2008), Three-dimensional crustal structure of the Mariana island arc from seismic tomography, *J. Geophys. Res.*, *113*, B01406, doi:10.1029/2007JB004939.

Caminos, R. (1979), Sierras Pampeanas Noroccidentales. Salta, Tucumán, Catamarca, La Rioja y San Juan, in *II Simposio de Geología Regional Argentina*, vol. 1, edited by E. F. Leanza, pp. 225–291, Acad. Nac. de Cienc. de Córdoba, Córdoba, Argentina.

Cawood, P. (2005), Terra Australis Orogen: Rodinia breakup and development of the Pacific and Iapetus margins of Gondwana during the Neoproterozoic and Paleozoic, *Earth Sci. Rev.*, *69*, 249–279, doi:10.1016/j.earscirev.2004.09.001.

Coira, B., B. Pérez, P. Flores, S. M. Kay, B. Woll, and M. Hanning (1999), Magmatic sources and tectonic setting of Gondwana margin Ordovician magmas,

northern Puna of Argentina and Chile, in *Laurentia-Gondwana Connections Before Pangea*, edited by V. Ramos and J. Keppie, *Spec. Pap. Geol. Soc. Am.*, *336*, 145–170.

Collo, G., R. A. Astini, A. Cardona, M. D. Do Campo, and U. Cordani (2008), Edades de metamorfismo en las unidades con bajo grado de la región central del Famatina: La impronta del ciclo orogénico oclóyico (Ordovícico), *Andean Geol.*, *35*, 191–213.

Cordani, U. G., L. M. Fraga, N. Reis, C. C. G. Tassinari, and B. B. Brito Neves (2010), On the origin and tectonic significance of the intra-plate events of Grenvillian-type age in South America: A discussion, *J. South Am. Earth Sci.*, *29*, 143–159, doi:10.1016/j.jsames.2009.07.002.

Davidson, J. P., and R. J. Arculus (2006), The significance of Phanerozoic arc magmatism in generating continental crust, in *Evolution and Differentiation of the Continental Crust*, edited by M. Brown and T. Rushmer, pp. 135–172, Cambridge Univ. Press, Cambridge, U. K.

DeBari, S. M. (1994), Petrogenesis of the Fiambala gabbroic intrusion, northwestern Argentina, a deep crustal syntectonic pluton in a continental magmatic arc, *J. Petrol.*, *35*, 679–713, doi:10.1093/petrology/35.3.679.

DeBari, S. M. (1997), Evolution of magmas in continental and oceanic arcs: The role of the lower crust, *Can. Mineral.*, *35*, 501–519.

de Brito Neves, B. B., and U. G. Cordani (1991), Tectonic evolution of South America during the late Proterozoic, *Precambrian Res.*, *53*, 23–40, doi:10.1016/0301-9268(91)90004-T.

DeCelles, P. G., M. N. Ducea, P. Kapp, and G. Zandt (2009), Cyclicity in Cordilleran orogenic systems, *Nat. Geosci.*, *2*, 251–257, doi:10.1038/ngeo469.

Depine, G. V., C. L. Andronicos, and J. Phipps-Morgan (2008), Near-isothermal conditions in the middle and lower crust induced by melt migration, *Nature*, *452*, 80–83, doi:10.1038/nature06689.

Drobe, M., M. López de Luchi, A. Steenken, R. Frei, R. Naumann, S. Siegesmund, and K. Wemmer (2009), Provenance of the late Proterozoic to early Cambrian metaclastic sediments of the Sierra de San Luis (eastern Sierras Pampeanas) and Cordillera Oriental, Argentina, *J. South Am. Earth Sci.*, *28*, 239–262, doi:10.1016/j.jsames.2009.06.005.

Ducea, M. N. (2001), The California arc: Thick granitic batholiths, eclogitic residues, lithospheric-scale thrusting, and magmatic flare-ups, *GSA Today*, *11*, 4–10, doi:10.1130/1052-5173(2001)011<0004:TCATGB>2.0.CO;2.

Ducea, M. N. (2002), Constraints on the bulk composition and root foundering rates of continental arcs: A California arc perspective, *J. Geophys. Res.*, *107* (B11), 2304, doi:10.1029/2001JB000643.

Ducea, M. N., and M. D. Barton (2007), Igniting flare-up events in Cordilleran arcs, *Geology*, *35*, 1047–1050, doi:10.1130/G23898A.1.

Ducea, M. N., S. Kidder, J. T. Chesley, and J. B. Saleeby (2009), Tectonic underplating of trench sediments beneath magmatic arcs: The central California example, *Int. Geol. Rev.*, *51*, 1–26, doi:10.1080/00206810802602767.

Fanning, C. M., R. J. Pankhurst, C. W. Rapela, E. G. Baldo, C. Casquet, and C. Galindo (2004), K-bentonites in the Argentine Precordillera contemporaneous with rhyolite volcanism in the Famatinian arc, *J. Geol. Soc. London*, *161*, 747–756, doi:10.1144/0016-764903-130.

Gehrels, G. E., V. A. Valencia, and J. Ruiz (2008), Enhanced precision, accuracy, efficiency, and spatial resolution of U-Pb ages by laser ablation-multicollector-inductively coupled plasma-mass spectrometry, *Geochem. Geophys. Geosyst.*, *9*, Q03017, doi:10.1029/2007GC001805.

Gehrels, G., et al. (2009), U-Pb geochronology of the Coast Mountains batholith in north-coastal British Columbia: Constraints on age and tectonic evolution, *Geol. Soc. Am. Bull.*, *121*, 1341–1361, doi:10.1130/B26404.1.

Greene, A. R., S. M. DeBari, P. K. Kelemen, J. Blustajn, and P. D. Clift (2006), A detailed geochemical study of island arc crust: The Talkeetna arc section, south-central Alaska, *J. Petrol.*, *47*, 1051–1093, doi:10.1093/petrology/egl002.

Hamilton, W. (1981), Crustal evolution by arc magmatism, *Philos. Trans. R. Soc. A*, *301*, 279–291.

Hoskin, P. W. O., and U. Schaltegger (2003), The composition of zircon and igneous and metamorphic petrogenesis, in *Zircon, Rev. Mineral. Geochem.*, vol. 53, edited by J. M. Hanchar and P. W. O. Hoskin, pp. 27–62, Mineral. Soc. of Am., Chantilly, Va.

Jagoutz, O., O. Müntener, P. Ulmer, T. Pettke, J.-P. Burg, H. Dawood, and S. Hussain (2007), Petrology and mineral chemistry of lower crustal intrusions: The Chilas complex, Kohistan (NW Pakistan), *J. Petrol.*, *48*, 1895–1953, doi:10.1093/petrology/egm044.

Ježek, P., A. P. Willner, F. G. Aceñolaza, and H. Miller (1985), The Puncoviscana trough—A large basin of late Precambrian to early Cambrian age on the Pacific edge of the Brazilian shield, *Geol. Rundsch.*, *74*, 573–584, doi:10.1007/BF01821213.

Jicha, B. R., D. W. Scholl, B. S. Singer, and G. M. Yogodzinski (2006), Revised age of Aleutian island arc formation implies high rate of magma production, *Geology*, *34*, 661–664, doi:10.1130/G22433.1.

Jicha, B. R., D. W. Scholl, and D. K. Rea (2009), Circum-Pacific arc flare-ups and global cooling near the Eocene-Oligocene boundary, *Geology*, *37*, 303–306, doi:10.1130/G25392A.1.

Jordan, T. E., and R. W. Allmendinger (1986), The Sierras Pampeanas of Argentina: A modern analog of Rocky-Mountain foreland deformation, *Am. J. Sci.*, *286*(10), 737–764.

Klepeis, K., G. L. Clarke, and T. Rushmer (2003), Magma transport and coupling between deformation and magmatism in the continental lithosphere, *GSA Today*, *13*, 4–11, doi:10.1130/1052-5173(2003)013<0004:MTACBD>2.0.CO;2.

Kretz, R. (1983), Symbols for rock-forming minerals, *Am. Mineral.*, *68*, 277–279.

Lackey, J. S., J. W. Valley, J. H. Chen, and D. F. Stockli (2008), Dynamic magma systems, crustal recycling, and alteration in the central Sierra Nevada batholith: The oxygen isotope record, *J. Petrol.*, *49*, 1397–1426, doi:10.1093/petrology/egn030.

Lipman, P. W. (2007), Incremental assembly and prolonged consolidation of Cordilleran magma chambers: Evidence from the southern Rocky Mountain volcanic field, *Geosphere*, *3*, 42–70, doi:10.1130/GES00061.1.

Ludwig, K. R. (2003), User's manual for Isoplot 3.00: A geochronological toolkit for Microsoft Excel, *Spec. Publ. 4*, 70 pp., Berkeley Geochronol. Cent., Berkeley, Calif.

Martino, R. D., A. B. Guereschi, and J. A. Sfragula (2009), Petrology, structure and tectonic significance of the Tuclame banded schists in the Sierras Pampeanas of Córdoba and its relationship with the metamorphic basement of northwestern Argentina, *J. South Am. Earth Sci.*, *27*, 280–298, doi:10.1016/j.jsames.2009.01.003.

Mirré, J. C. (1976), Descripción geológica de la Hoja 19e, Valle Fértil, provincias de San Juan y La Rioja, report, pp. 1–70, Serv. Geol. Nac., Buenos Aires.

Mulcahy, S. R., S. M. Roeske, W. C. McClelland, S. Nomade, and P. R. Renne (2007), Cambrian initiation of the Las Pirquitas thrust of the western Sierra Pampeanas, Argentina: Implications for the evolution of the proto-Andean margin of South America, *Geology*, *35*, 443–446, doi:10.1130/G23436A.1.

Murra, J. A., and E. G. Baldo (2004), Condiciones de emplazamiento de la granodiorita Valle Fértil y su comparación con el batolito de Los Llanos-Ulapes, in *Avances en Mineralogía, Metalogenia y Petrología*, edited by M. Brodtkorb et al., pp. 367–372, Asociación Mineralógica Argentina, Buenos Aires.

Otamendi, J. E., A. M. Tibaldi, G. I. Vujovich, and G. A. Viñao (2008), Metamorphic evolution of migmatites from the deep Famatinian arc crust exposed in Sierras Valle Fértil-La Huerta, San Juan, Argentina, *J. South Am. Earth Sci.*, *25*, 313–335, doi:10.1016/j.jsames.2007.09.001.

Otamendi, J. E., G. I. Vujovich, J. D. de la Rosa, A. M. Tibaldi, A. Castro, R. D. Martino, and L. P. Pinotti (2009a), Geology and petrology of a deep crustal zone from the Famatinian paleo-arc, Sierras Valle Fértil-La Huerta, San Juan, Argentina, *J. South Am. Earth Sci.*, *27*, 258–279, doi:10.1016/j.jsames.2008.11.007.

Otamendi, J. E., M. N. Ducea, A. M. Tibaldi, G. Bergantz, J. D. de la Rosa, and G. I. Vujovich (2009b), Generation of tonalitic and dioritic magmas by coupled partial meting of gabbroic and metasedimentary migmatites in the deep crust of the Famatinian arc Argentina, *J. Petrol.*, *50*, 841–873, doi:10.1093/petrology/egp022.

Pankhurst, R. J., C. W. Rapela, J. Saavedra, E. G. Baldo, J. Dahlquist, I. Pascua, and C. M. Fanning (1998), The Famatinian magmatic arc in the central Sierras Pampeanas: An early to mid-Ordovician continental arc on the Gondwana margin, in *The Proto-Andean Margin of Gondwana*, edited by R. J. Pankhurst and C. W. Rapela, *Geol. Soc. Spec. Publ.*, *142*, 343–368.

Pankhurst, R. J., C. W. Rapela, and C. M. Fanning (2000), Age and origin of coeval TTG, I- and S-type granites in the Famatinian belt of NW Argentina, *Trans. R. Soc. Edinburgh Earth Sci.*, *91*, 151–168.

Piñán-Llamas, A., and C. Simpson (2006), Deformation of Gondwana margin turbidites during the Pampean orogeny, north-central Argentina, *Geol. Soc. Am. Bull.*, *118*, 1270–1279, doi:10.1130/B25915.1.

Pitcher, W. S. (1993), *The Nature and Origin of Granite*, 321 pp., Chapman and Hall, London.

Ramos, V. A. (2004), Cuyania, an exotic block to Gondwana: Review of a historical success and the present problems, *Gondwana Res.*, *7*, 1009–1026, doi:10.1016/S1342-937X(05)71081-9.

Ramos, V. A. (2008), The basement of the central Andes: The Arequipa and related terranes, *Annu. Rev. Earth Planet. Sci.*, *36*, 289–324, doi:10.1146/annurev.earth.36.031207.124304.

Rapela, C. W., B. Coira, A. Toselli, and J. Saavedra (1992), The lower Paleozoic magmatism of southwestern Gondwana and the evolution of Famatinian orogen, *Int. Geol. Rev.*, *34*, 1081–1142, doi:10.1080/00206819465657.

Rapela, C. W., R. J. Pankhurst, C. Casquet, E. G. Baldo, J. Saavedra, C. Galindo, and C. M. Fanning (1998), The Pampean orogeny of the southern proto-Andes: Cambrian continental collision in the Sierras de Córdoba, in *The Proto-Andean Margin of Gondwana*, edited by R. J. Pankhurst and C. W. Rapela, *Geol. Soc. Spec. Publ.*, *142*, 181–207.

Rapela, C. W., R. Pankhurst, E. Baldo, C. Casquet, C. Galindo, C. Fanning, and J. Saavedra (2001), Ordovician metamorphism in the Sierras Pampeanas: New U-Pb SHRIMP ages in central-east Valle Fértil and the Velasco batholith, paper presented at III South American Symposium on Isotope Geology, Argent. Geol. Soc., Buenos Aires.

Rapela, C. W., R. J. Pankhurst, C. Casquet, C. M. Fanning, E. G. Baldo, J. M. González-Casado, C. Galindo, and J. Dahlquist (2007), The Río de la Plata craton and the assembly of SW Gondwana, *Earth Sci. Rev.*, *83*, 49–82, doi:10.1016/j.earscirev.2007.03.004.

Reymer, A., and G. Schubert (1984), Phanerozoic addition rates to the continental-crust and crustal growth, *Tectonics*, *3*, 63–77, doi:10.1029/TC003i001p00063.

Saleeby, J., M. N. Ducea, and D. Clemens-Knott (2003), Production and loss of high-density batholithic root, southern Sierra Nevada, California, *Tectonics*, *22*(6), 1064, doi:10.1029/2002TC001374.

Schwartz, J. J., L. P. Gromet, and R. Miró (2004), Provenance of a late Proterozoic–early Cambrian basin,

Sierras de Córdoba, Argentina, *Precambrian Res.*, *129*, 1–21, doi:10.1016/j.precamres.2003.08.011.

Schwartz, J. J., L. P. Gromet, and R. Miró (2008), Timing and duration of the calc-alkaline ac of the Pampean orogeny: Implications for the late Neoproterozoic to Cambrian evolution of western Gondwana, *J. Geol.*, *116*, 39–61, doi:10.1086/524122.

Stacey, J. S., and J. D. Kramers (1975), Approximation of terrestrial lead isotope evolution by a two-stage model, *Earth Planet. Sci. Lett.*, *26*, 207–221, doi:10.1016/0012-821X(75)90088-6.

Steenken, A., S. Siegesmund, M. G. López de Luchi, R. Frei, and K. Wemmer (2006), Neoproterozoic to early Palaeozoic events in the Sierra de San Luis: Implications for the Famatinian geodynamics in the eastern Sierras Pampeanas (Argentina), *J. Geol. Soc.*, *163*, 965–982, doi:10.1144/0016-76492005-064.

Thomas, W. A., and R. A. Astini (1996), The Argentine Precordillera: A traveler from the Ouachita embayment of North American Laurentia, *Science*, *273*, 752–757, doi:10.1126/science.273.5276.752.

Toselli, A. J., F. R. Durand, J. N. Rossi de Toselli, and J. Saavedra (1996), Esquema de evolución geotectónica y magmática Eopaleozoica del sistema de Famatina y sectores de Sierras Pampeadas, paper presented at XIII Congreso Geológico Argentino y III Congreso de Exploración de Hidrocarburos, Argent. Geol. Soc., Buenos Aires.

Trompette, R. (1997), Neoproterozoic (~600 Ma) aggregation of western Gondwana: A tentative scenario, *Precambrian Res.*, *82*, 101–112, doi:10.1016/S0301-9268(96)00045-9.

von Huene, R., and D. W. Scholl (1991), Observations at convergent margins concerning sediment subduction, subduction erosion and the growth of continental crust, *Rev. Geophys.*, *29*, 279–316, doi:10.1029/91RG00969.

Vujovich, G. I., M. Godeas, G. Marín, and N. Pezzutti (1996), El complejo magmático de la Sierra de La Huerta, provincia de San Juan, paper presented at XIII Congreso Geológico Argentino y III Congreso de Exploración de Hidrocarburos, Argent. Geol. Soc., Buenos Aires.

Zeng, L., J. Saleeby, and M. N. Ducea (2005), Geochemical characteristics of crustal anatexis during the formation of migmatite at the southern Sierra Nevada, California, *Contrib. Mineral. Petrol.*, *150*, 386–402, doi:10.1007/s00410-005-0010-2.

Zimmermann, U. (2005), Provenance studies of very low to low-grade metasedimentary rocks of the Puncoviscana complex, northwest Argentina, in *Terrane Processes at the Margins of Gondwana*, edited by A. P. M. Vaughan, P. T. Leat, and R. J. Pankhurst, *Geol. Soc. Spec. Publ.*, *246*, 381–416.

G. Bergantz, Department of Earth and Space Sciences, University of Washington, Seattle, WA 98195, USA.

M. N. Ducea, G. E. Gehrels, K. M. Stair, and V. A. Valencia, Department of Geosciences, University of Arizona, Tucson, 85721 AZ, USA. (ducea@email.arizona.edu)

J. E. Otamendi, Departamento de Geología, Univesidad Nacional de Río Cuarto, X5804 Río Cuarto, Argentina.